Received 15 May 2024; revised 17 June 2024; accepted 10 July 2024. Date of publication 16 July 2024; date of current version 29 July 2024.

*Digital Object Identifier 10.1109/OJCOMS.2024.3428925*

# Backhaul-Aware UAV-Aided Capacity Enhancement in Mixed FSO-RF Network

**MUHAMMAD NAFEES (Member, IEEE), SHENJIE HUANG (Member, IEEE), JOHN THOMPSON (Fellow, IEEE), AND MAJID SAFARI (Senior Member, IEEE)**

School of Engineering, Institute for Imaging, Data and Communications, The University of Edinburgh, EH9 3JL Edinburgh, U.K.

CORRESPONDING AUTHOR: M. NAFEES (e-mail: m.nafees@ed.ac.uk)

The work of Majid Safari and Shenjie Huang was supported by the Engineering and Physical Sciences Research Council (EPSRC) through the Terabit Bidirectional Multi-User Optical Wireless System (TOWS) for 6G LiFi under Grant EP/S016570/2.

**ABSTRACT** Future networks are expected to make substantial use of unmanned aerial vehicles (UAVs) as aerial base stations (BSs). The backhauling of UAVs is often considered with license-free and high-bandwidth free-space optical (FSO) communication. Employing UAVs and FSO technology together is appropriate for numerous applications such as user offloading, network capacity enhancement, and relaying services. However, the reliability of the backhaul FSO link can be jeopardized by infrequent adverse weather conditions such as fog. In this study, we proposed the capacity enhancement of a ground BS (GBS) with the aid of an FSO-backhualed UAV aerial BS. In particular, we optimize the UAV's circular trajectory and parameters (i.e., coverage radius and beamwidth) to maximize the total network throughput during both normal and adverse weather (e.g., fog events). Two trajectories, namely rate maximization (RMT) and fairness-constrained rate maximization (FRMT), are considered. A novel expression for the average capacity of the FSO backhaul over the entire trajectory is derived. The formulated problem aims to maximize the average network throughput with constraints pertaining to backhaul capacity, network fairness, and UAV parameters. It is shown that the UAV changes its trajectory using its coverage radius and directional antenna beamwidth according to the weather conditions and fairness requirements to maximize the total system capacity. Furthermore, real weather data from the cities of Edinburgh and London in the U.K. is used to evaluate the performance of the system under low-visibility conditions. The numerical results show the proposed FSO-backhauled UAV can provide significant capacity enhancement even in thin, light, and moderately foggy conditions.

**INDEX TERMS** Beyond fifth-generation (B5G), free-space optical (FSO) communication, millimeter wave (mmWave), unmanned aerial vehicle (UAV).

## I. INTRODUCTION

THE MARKET for commercial unmanned aerial vehicles (UAVs) is expected to reach over 13 billion U.S. dollars by 2025 [1]. Due to their unlimited 3D mobility and autonomous flight capabilities, UAVs are envisioned to be increasingly used in future wireless networks [2]. In addition, beyond fifth-generation (B5G) wireless networks are projected to address many of the limitations of current wireless infrastructure by increasing data speeds, improving quality-of-service (QoS) in congested areas, and diminishing current network blind spots. For the sake of achieving increased system capacity, free-space optical (FSO) communication is predicted to play a critical role in B5G wireless networks [3]. Because of their ease of deployment, quick setup time, and cheap maintenance costs, FSO links are a possible alternative to traditional fiber optics used for backhaul connectivity. Furthermore, in the context of B5G, the combination of FSO communication and UAVs is a key component in a variety of high-data-rate application scenarios [4], [5], [6].

Practical FSO systems face challenges such as pointing and misalignment loss caused by building sways, unpredictable connectivity in the presence of the atmosphere due to turbulence-induced intensity fluctuation (scintillation), and bad weather such as snow and fog [7]. The fog events are relatively long-lasting, which may necessitate changes and alternative solutions to the regular use of FSO links. A UAV

aerial BS is typically considered with an ideal FSO backhaul in the literature [3], [8]. In frequent good weather conditions, the FSO links are very reliable and offer high-speed backhaul connectivity. However, due to adverse weather effects on the backhaul link, UAV aerial BS might need to change its fixed position or trajectory so that the adverse weather's impact on its FSO backhaul links can be minimized to improve the performance of the network in many scenarios. Mixed FSO-radio frequency (RF) relaying systems have been widely deployed in static deployment scenarios [9], [10]. A combination of FSO and millimeter wave (mmWave) in the backhaul and access links, respectively, for the UAV aerial BS is also often employed. To this end, the coverage and trajectory of UAVs for providing high-quality capacity enhancement adhering to their backhaul capacity is one of the main challenges for the implementation of future wireless systems, and this constitutes the main subject of this study. Note that this paper considers a fixed-wing UAV, known for its superior endurance in flight compared to rotary-wing counterparts. While energy consumption is not the primary focus of this paper, any tradeoffs between trajectory time and power consumption are disregarded. It is assumed that the UAV could be refueled or replaced at intervals, allowing the investigation to focus on trajectory optimization for capacity enhancement without considering these tradeoffs.

### A. RELATED WORK

Backhaul optimization and the related user association issues have recently attracted significant attention from the research community. This is because it is anticipated that the key bottleneck in B5G networks is going to shift from access to backhaul links [11]. Studies on optimal UAV deployment have largely ignored the backhauling problem (e.g., [12]), as most of the literature on UAV-assisted networks assumes an ideal FSO backhaul or pays no attention to the backhaul problems. In [13], for example, 3D UAV deployment and resource allocation are performed for a hotspot region to maximize access link throughput while taking user QoS, backhaul link capacity, system bandwidth, and power into account. However, assuming the FSO link's capacity is high enough in clear weather, it's excluded from the optimization problem. Some studies [14], [15] have assumed an ideal FSO backhaul or considered the backhaul as a future study. The study in [16] considered a backhaul-aware resource allocation problem in a UAV-to-everything network; however, the main focus is on resource allocation in a layered framework, which can help determine the optimal number of transfers among UAVs and save energy while enhancing resource allocation performance.

One of the key research areas in UAV-aided wireless networks is UAV trajectory optimization. For instance, a multi-UAV trajectory scheme is proposed in [17] that develops optimal UAV trajectories to maximize service time between users and UAVs in an FSO-based wireless aerial system with multiple users and UAVs. To offload traffic for BSs, the study in [18] emphasized the UAV trajectory at the boundaries of three neighboring cells. By optimizing the UAV trajectory in each flight cycle, the proposed system maximizes the cumulative rate of UAV-served edge users while still meeting the rate requirements for all users. In [19], a UAV with a configurable directional antenna beamwidth is used to distribute a shared file to a group of ground users. The authors studied how beamwidth control impacts the UAV's 3D location and trajectory by minimizing mission completion time. The UAV trajectory and network resource allocation are jointly optimized in [14] for a wireless network consisting of an UAV aerial BS with a directional antenna and a terrestrial BS to maximize the minimum throughput of mobile terminals. An algorithm combining optimal trajectory design and a resource allocation mechanism is developed in [20] to accomplish the data collection task with the minimum energy consumed both by ground users and the UAV. With an objective to maximize the sum rate, the study in [21] proposed an iterative technique to optimize the UAV's trajectory to the deployment location, which involves the UAV iteratively searching for the optimal location. The work in [8] proposed a trajectory optimization approach for an FSO-based UAV-Internet-of-Things (IoT) backhaul network scheme that minimizes the end-to-end outage probability considering moving clouds and obstacles. In [22], the authors propose deploying a relaying node to obtain LoS when barriers, such as buildings, exist between the source and destination. However, the primary goal of this research is to determine the ideal location of the UAV relay while taking into account physical criteria such as height and the position of obstacles. In [23], a recent study discusses the design of a multi-layer airborne backhaul network using UAVs with FSO links for global coverage in future networks. However, the study focuses solely on trajectory design based on circular tracks for multiple UAVs without considering the impact of trajectory on FSO channel capacity.

There are several studies (e.g., [29]) that have considered the impact of weather on the fixed FSO backhaul links. The impact of weather on FSO or other backhaul networks employing UAV-aided offloading and capacity enhancement has almost received no attention. For instance, the study in [30] investigated how different weather conditions affect the vertical FSO link between the UAV and the GBS. However, the UAV's movement and trajectory are not taken into account, and the impact of fog attenuation is also neglected. The study in [31] proposed a complementary solution to terrestrial applications with the goal of developing a scalable and cost-effective FSO-RF system for 5G communication. However, this work disregards the movement and trajectory design of the UAV and instead concentrates on point-to-point backhauling between the UAV and access point. Research in [24] considered an UAV-aided FSO communication for the trajectory optimization for the flight time maximization. However, average backhaul capacity is not considered in this research. Instead, the focus is on service time, which is based on meeting a minimum data rate

**TABLE 1.** The key insights in recent trajectory-based UAV-aided network research for RF and hybrid networks: notable works and related references.

| Trajectory | Backhaul | Objective | Network | Ref. |
|---|---|---|---|---|
| Circular | Discrete-time rate model | Trajectory optimization for FSO based UAV-IoT (U-IoT) backhaul network | Mixed FSO-RF | [8] |
| Circular | Assumed to be ideal | Maximization of the minimum throughput of all users by optimizing the UAV's trajectory, bandwidth allocation, and user partitioning | RF-only | [14] |
| Circular, non-circular | Discrete-time rate model | Trajectory optimization for flight time maximization | Mixed FSO-RF | [24] |
| Circular | Assumed to be ideal | UAV detection and localization based on multi-dimensional signal features | RF-only | [25] |
| Circular | Assumed to be ideal | Energy-efficient communication for UAV-enabled mobile relay networks | RF-only | [26] |
| Non-circular | Discrete-time rate model | Optimizing UAV trajectory to avoid clouds for enhanced connection time in UAV to BS communication | FSO-only | [27] |
| Non-circular | Assumed to be ideal | Maximization of minimum rate and enhance user fairness while considering the available on-board energy | RF-only | [28] |

threshold. In a more recent study [32], FSO technology is employed as the backhaul solution to significantly improve the link capacity between a macro base station (MBS) and a UAV with backhaul constraints. However, the study focuses on a hovering UAV-based deployment over a cluster of users without a UAV trajectory, with a focus on bandwidth allocation and UAV placement optimization, including the impact of weather on UAV altitude and the satisfaction of users. Table 1 summarizes some closely related works involving trajectory optimization with UAV networks. One can note that backhaul considerations are typically based either on a discrete-time model or on the assumption of an ideal backhaul link.

### B. OBJECTIVES AND CONTRIBUTIONS

In this paper, capacity enhancement of a network served by a ground BS (GBS) is performed with the aid of a UAV aerial BS. The GBS serves its users using the sub-6 GHz spectrum, whereas the UAV has high-speed backhaul and access links using FSO technology and mmWave technology. Since the end-to-end system capacity is influenced by both the backhaul and access links, a backhaul-aware UAV trajectory optimization is performed, and the impact of good and adverse weather on the UAV's trajectory is evaluated. In particular, the effect of the FSO backhaul capacity limit on the UAV trajectory is evaluated using orthogonal spectra of sub-6 GHz and mmWave for the GBS and UAV aerial BS, respectively. A novel expression for the average backhaul capacity for the FSO link is derived. Since the impact of the UAV's trajectory should be reflected in the total network performance (e.g., system fairness), it is inevitable to involve GBS's network throughput in the problem. This renders the final problem exceedingly challenging to solve using standard optimization techniques. Hence, to solve the optimization problem efficiently, a powerful technique known as the whale optimization algorithm (WOA) is used. In the proposed system, the UAV's trajectory can be optimized in view of the fairness requirement and the changing weather conditions. Our main contributions are summarized as follows:

- This study optimizes the FSO backhaul-aware trajectory of the UAV, which supports the GBS, to enhance the capacity of the network in the context of B5G networks. A novel mathematical expression for the average backhaul capacity of the UAV-aided FSO link's circular trajectory is derived. The average FSO backhaul capacity expression allows an on-board UAV buffer to compensate for the time-varying access and backhaul link data rates.
- The UAV's circular trajectory in 3D space is adjusted to improve the system throughput by optimizing its antenna beamwidth and coverage radius according to weather attenuation conditions and fairness requirements. Two backhaul-constrained objectives, namely the sum-**r**ate **m**aximization **t**rajectory (RMT) and the **f**airness-constrained sum-**r**ate **m**aximization **t**rajectory (FRMT), are considered.
- The extensive numerical results demonstrate that the UAV's circular trajectory could be substantially changed by the reliability of its FSO backhaul and system fairness requirements. In terms of reliability, this change is most noticeable in adverse weather conditions. Additionally, user QoS (e.g., fifth-percentile throughput) and network sum-rate exhibit an intriguing tradeoff.
- The proposed system is also tested using real-world meteorological data from Edinburgh and London. The results reveal that the UAV can effectively increase user data rates and network capacity in foggy channel conditions.

The rest of this paper is organized as follows: The system model of the proposed UAV-aided mixed FSO-RF network is presented in Section II. The trajectory optimization for maximizing the network throughput is detailed in Section III. Some numerical results and the results based on practical measurements are provided in Sections IV and V, respectively. Finally, the paper is concluded in Section VI.

## II. SYSTEM MODEL AND UAV TRAJECTORY

This paper considers a single-cell wireless communication system with a GBS centered at the origin of a coverage

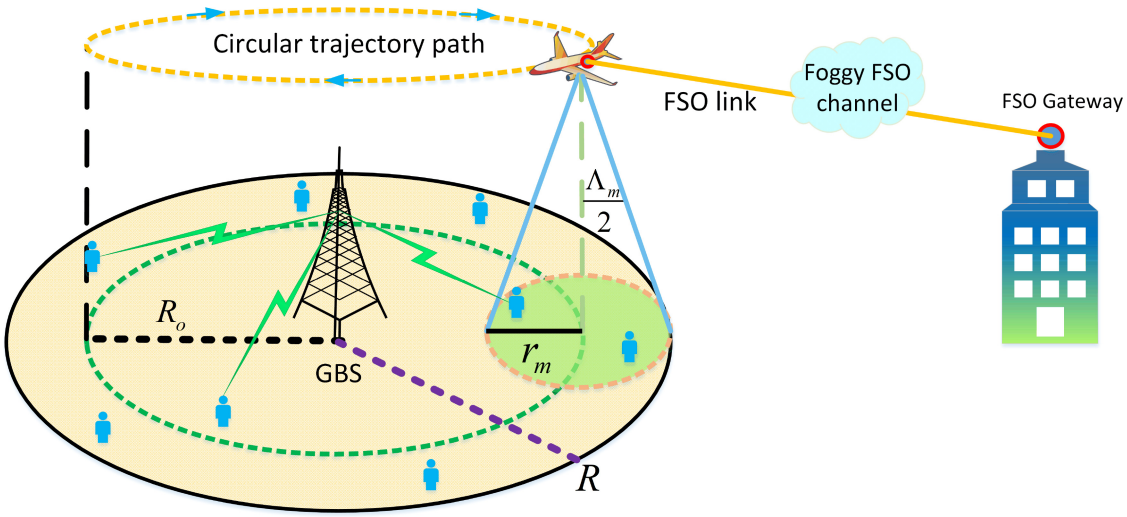


**FIGURE 1.** System model for the circular UAV trajectory for network capacity enhancement with FSO backhaul.

area of radius $R$. The $K$ number of users is distributed uniformly and randomly throughout the cell. In the context of B5G, a mmWave and sub-6 GHz dual-mode network (e.g., [33], [34]) is considered, which can take advantage of the signals over both bands. The GBS serves all the users with sub-6 GHz access links, whereas a fixed-wing UAV acting as an aerial BS is employed to serve a portion of the cell with mmWave access links for the QoS enhancement of the users, as illustrated in Fig. 1. We consider a simple frequency division multiple access (FDMA)-inspired resource allocation policy under which the total access bandwidth is shared equally among its associated users [35]. Note that we consider the FDMA-based scheme as it can be efficiently mapped into corresponding orthogonal FDMA-based allocations involving frequency band partitioning into multiple physical resource blocks [36]. Also, it is considered that the UAV has an FSO backhaul to a nearby FSO gateway $\mathcal{G}$. Note that a circular UAV trajectory model (e.g., [14], [37]) is considered in this paper, wherein the UAV footprint is always tangential to the edge of the cell from inside. That is, the coverage footprint of the UAV aerial BS increases as the UAV moves closer to the origin of the coverage area. Consider that the UAV flies in a cyclic manner above the cell with a constant cycle flight time $T$, which can be discretized into $N$ equal time slots. It is considered that the UAV periodically serves a portion of users with a coverage radius of $r_m$, assuming a homogeneous and rotationally symmetric beam pattern [38]. The FSO gateway is considered to be located at $[x_{\mathcal{G}}, y_{\mathcal{G}}, h_{\mathcal{G}}] \in \mathbb{R}^{3\times 1}$ at a distance $d_{\mathcal{G}}$ from the origin of the GBS's coverage area. Then, the time-varying position of the UAV is denoted as $[x_m[n], y_m[n], h_m[n]]^T$, $n = 1, 2, \ldots, N$. The circular serving region of the UAV aerial BS is defined by its coverage radius and the trajectory radius (from the origin), denoted by $r_m$ and $R_o$, respectively.

When fog events occur, the UAV aerial BS's FSO backhaul might be greatly impacted, and the UAV might want to alter its coverage trajectory, e.g., changing coverage radius or altitude, to minimize the attenuation on the FSO backhaul link induced by the adverse weather conditions. Also, the UAV's circular trajectory might be impacted by the network QoS requirements for its users. Note that the backhaul capacity of the UAV varies due to the change in distance from the FSO gateway $\mathcal{G}$ during the circular trajectory, which can cause disparity in the offered data rates to the network users, especially in adverse conditions. To this end, an average FSO backhaul capacity expression is derived in the following section.

### A. UAV BACKHAUL CAPACITY

When intensity modulation direct detection (IM/DD) is used in the FSO link, the received electrical signal may be expressed as

$$s_{\mathrm{o}} = \rho g_{\mathrm{o}} h_{\mathrm{o}} x_{\mathrm{o}} + z_{\mathrm{o}}, \tag{1}$$

where $\rho$ denotes the responsivity of the photo-detector, $g_{\mathrm{o}}$ is the average gain to the receiver optical power, $x_{\mathrm{o}}$ refers to the transmitted optical intensity, $s_{\mathrm{o}}$ represents the received electrical signal, and the zero-mean real Gaussian noise with variance $\sigma_{\mathrm{o}}^2$ is denoted by $z_{\mathrm{o}}$. Note that an advanced pointing, acquisition, and tracking (PAT) method is assumed to be capable of compensating for pointing errors [39]. Numerous studies, such as those highlighted by [40], offer a range of solutions addressing the PAT challenges between a mobile UAV and a stationary FSO gateway. Research such as [41] has demonstrated that PAT between a UAV and an FSO node can adaptively function under various weather conditions. Additionally, there is an inverse correlation between atmospheric turbulence and fog [42], [43], [44]. Various turbulence mitigation solutions have been proposed, including pulse position modulation [45], the use of concave mirrors [46], adaptive optics correction [47], and turbulence-resistant few-mode pre-amplified receivers [48], each tailored

to different scenarios for mitigating the impact of turbulence. Research [49] suggests that the average impact of turbulence-induced intensity fading can be simplified to unity, i.e., $\mathbb{E}[h_o] = 1$. Other studies, such as [24], completely ignore the impact of both turbulence and pointing errors to focus on other aspects. Therefore, in this analysis, turbulence-induced intensity fading $h_o$ is ignored to evaluate the average FSO backhaul capacity. The average gain $g_o$ can be expressed as[50]

$$g_o = \frac{A}{\pi\left(\frac{\varpi}{2} d_{\mathcal{B}}\right)^2} \exp^{-(\vartheta d_{\mathcal{B}})}, \tag{2}$$

where $A = \pi(\frac{\gamma}{2})^2$, the first and second terms represent geometric and weather-related atmospheric losses owing to scattering and absorption, respectively. Wherein the diameter of the receiver aperture is denoted by $\gamma$, $\varpi$ represents the beam divergence angle, $d_{\mathcal{B}}$ shows the point-to-point link distance from the FSO gateway to the destination (UAV location), and $\vartheta$ is a weather-dependent attenuation coefficient determined based on the Beer-Lambert law. The attenuation coefficient $\vartheta$ and the visibility $V$ in km are related as $\vartheta = \frac{3.91}{V}(\frac{\lambda_o}{550\times10^{-9}})^{-\xi}$, where $\lambda_o$ is the optical wavelength and $\xi$ is the weather condition-based size distribution of the scattering particles. It is defined as a function of visibility distance as [51]

$$\xi = \begin{cases} 1.6, & V > 50\,\text{km} \\ 1.3, & 6\,\text{km} < V < 50\,\text{km} \\ 0.16V + 0.34, & 1\,\text{km} < V < 6\,\text{km} \\ V - 0.5, & 0.5\,\text{km} < V < 1\,\text{km} \\ 0, & V < 0.5\,\text{km}. \end{cases} \tag{3}$$

We adopt the FSO channel capacity model used in [13], [52], and based on (1), the achievable backhaul rate of the FSO link for a given UAV position during its circular trajectory $\mathcal{T}$ is given by

$$C_{\mathcal{T}} = \frac{1}{2} W_o \log_2\left(1 + \frac{e\zeta_o^2 g_o^2 \rho^2}{2\pi\sigma_o^2}\right), \tag{4}$$

where $W_o$ denotes the bandwidth of the FSO link, $e$ is the base of the natural logarithm, and $\zeta_o$ represents the optical transmission power. Substituting (2) into (4), we have

$$C_{\mathcal{T}} = \frac{W_o}{2} \log_2\left(1 + \frac{e\rho^2\gamma^4\zeta_o^2 \exp^{-(2\vartheta d_{\mathcal{B}})}}{2\pi\sigma_o^2\varpi^4 d_{\mathcal{B}}^4}\right), \tag{5}$$

consider $\mathcal{W}_o = \frac{e\rho^2\gamma^4\zeta_o^2}{2\pi\sigma_o^2\varpi^4}$ represents the constant terms, then (5) can be simplified as

$$C_{\mathcal{T}} = \frac{W_o}{2} \log_2\left(1 + \frac{\mathcal{W}_o \exp^{-(2\vartheta d_{\mathcal{B}})}}{d_{\mathcal{B}}^4}\right). \tag{6}$$

In order to address the challenges in asymmetric dual-hop relay systems (e.g., dual-hop relay transmission with mixed FSO-RF links), it is practical to include buffering for relaying [53]. Hence, it is assumed that the UAV is equipped with a buffer for temporarily storing data, leading to the objective of calculating the average capacity of the UAV's backhaul link over its complete circular trajectory. However, as illustrated in Fig. 2, the link distance between the FSO gateway and the UAV does not linearly change, which makes it hard to calculate the average capacity. One can note that the link distance can be translated into the angular motion of the UAV. Then, the UAV backhaul link distance, i.e., UAV to gateway distance $d_{\mathcal{B}}$, as illustrated in Fig. 2, can be calculated as follows

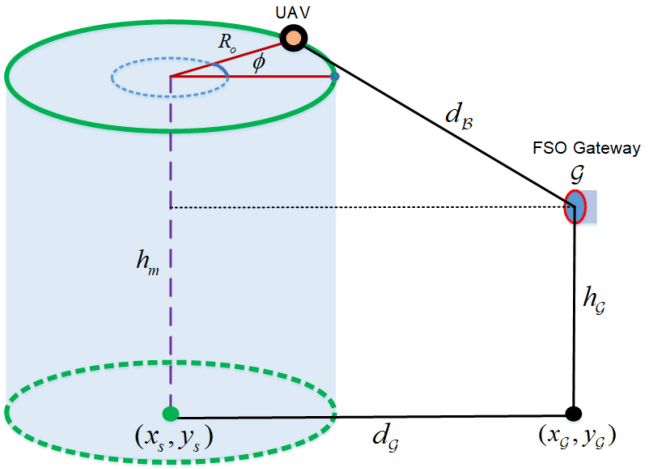


**FIGURE 2.** Representation of changing distance with angle $\phi$ between UAV and the FSO gateway $\mathcal{G}$.

$$d_{\mathcal{B}}(\phi) = \sqrt{h_{\bar{m}}^2 + d_{\mathcal{G}}^2 + R_o^2 - 2d_{\mathcal{G}}R_o\cos(\phi)}, \tag{7}$$

where $h_{\bar{m}} = (h_m - h_{\mathcal{G}})$, $d_{\mathcal{G}} = \sqrt{(x_{\mathcal{G}} - x_s)^2 + (y_{\mathcal{G}} - y_s)^2}$ is the ground distance from the center of the coverage region $(x_s, y_s)$ to the center of the FSO gateway $(x_{\mathcal{G}}, y_{\mathcal{G}})$, and $R_o = (R - r_m)$ is the UAV trajectory radius with UAV coverage radius $r_m$.

Now, using the channel capacity in (6), the average channel capacity over the entire circular trajectory $\mathcal{T}$ of the UAV can be written in the integral form as

$$\overline{C_{\mathcal{T}(\phi)}} = W_o \times \frac{1}{2\pi}\int_0^{\pi} \log_2\left(1 + \frac{\mathcal{W}_o \exp\left(-2\vartheta\sqrt{\mathscr{X} - \mathscr{Y}\cos(\phi)}\right)}{\left[\mathscr{X} - \mathscr{Y}\cos(\phi)\right]^2}\right) d\phi, \tag{8}$$

where $\mathscr{X} = (h_{\bar{m}}^2 + d_{\mathcal{G}}^2 + R_o^2)$ and $\mathscr{Y} = 2d_{\mathcal{G}}R_o$. For the sake of mathematical simplicity, we can disregard the constant term 1 in the logarithmic expression of (8), leading to a capacity lower bound as

$$\overline{C_{\mathcal{T}(\phi)}} = W_o \times \frac{1}{2\pi}\int_0^{\pi} \log_2\left(\frac{\mathcal{W}_o \exp\left(-2\vartheta\sqrt{\mathscr{X} - \mathscr{Y}\cos(\phi)}\right)}{\left[\mathscr{X} - \mathscr{Y}\cos(\phi)\right]^2}\right) d\phi, \tag{9}$$

by using the properties of integrals, we can write (9) as

$$\overline{C}_{\mathcal{T}} = \frac{W_o}{2}\log_2(\mathcal{W}_o) - \frac{W_o}{\pi}\vartheta\log_2(e)\underbrace{\int_0^{\pi}\sqrt{\mathscr{X}-\mathscr{Y}\cos(\phi)}d\phi}_{\mathcal{I}_1} - \frac{W_0}{\pi}\underbrace{\int_0^{\pi}\log_2(\mathscr{X}-\mathscr{Y}\cos(\phi))d\phi}_{\mathcal{I}_2}. \tag{10}$$

According to [54, eq. (3.670.1)], the integral $\mathcal{I}_1$ can be expressed as

$$\mathcal{I}_1 = 2\sqrt{\mathscr{X}+\mathscr{Y}}\mathbb{K}\left(\sqrt{\frac{2\mathscr{Y}}{\mathscr{X}+\mathscr{Y}}}\right), \tag{11}$$

where $\mathbb{K}(\cdot)$ denotes the complete elliptic integral of the first kind. Also, using [54, eq. (4.224.9)], the integral $\mathcal{I}_2$ can be solved as

$$\mathcal{I}_2 = \frac{\pi}{\ln 2}\ln\left(\frac{\mathscr{X}+\sqrt{\mathscr{X}^2-\mathscr{Y}^2}}{2}\right), \tag{12}$$

finally, the average backhaul capacity for the UAV aerial BS's complete circular trajectory can be expressed as

$$\overline{C}_{\mathcal{T}} = \frac{W_o}{2}\log_2(\mathcal{W}_o) - \frac{W_o}{\pi}2\vartheta\log_2 e\sqrt{\mathscr{X}+\mathscr{Y}} \times \mathbb{K}\left(\sqrt{\frac{2\mathscr{Y}}{\mathscr{X}+\mathscr{Y}}}\right) - \frac{W_o}{\ln 2}\ln\left(\frac{\mathscr{X}+\sqrt{\mathscr{X}^2-\mathscr{Y}^2}}{2}\right). \tag{13}$$

As stated above, the average channel capacity $\overline{C}_{\mathcal{T}}$ is derived without accounting for turbulence-induced intensity fluctuations. This assumption is reasonable, as foggy conditions are typically associated with weak to moderate turbulence. In Section IV, we numerically demonstrate that this derived capacity remains a reliable approximation under these turbulence conditions.

### B. UAV-USER COMMUNICATION

Though line-of-sight (LoS) communications dominate UAV-user channels [14], [55], the significance of non-LoS (NLoS) transmission, particularly in urban contexts, cannot be ignored. Therefore, the channel between the UAV and the users consists of both LoS and NLoS components. The probability of a LoS link between the UAV and the $k$th user could be stated as

$$P_{\mathrm{m}k}^{\mathrm{LoS}}(\theta_k) = \frac{1}{1+\omega_1\exp\big(-\omega_2[\theta_k-\omega_1]\big)}, \tag{14}$$

where $\omega_1$ and $\omega_2$ are constant parameters that depend on carrier frequency and the communication environment, and $\theta_k = \frac{180}{\pi}\times\sin^{-1}(\frac{h_{\mathrm{m}}}{d_{\mathrm{m}k}})$ is the elevation angle between the $k$th user and the UAV with $d_{\mathrm{m}k} = \sqrt{(x_{\mathrm{m}}-x_k)^2+(y_{\mathrm{m}}-y_k)^2+h_{\mathrm{m}}^2}$, the distance between the $k$th user and the UAV, which has an altitude of $h_{\mathrm{m}}$. Then, path loss (PL) for the LoS and NLoS links could be stated as [56]

$$\begin{cases}\mathcal{L}_{\mathrm{m}k}^{\mathrm{LoS}} = \Gamma_1\left(\frac{4\pi f_{\dot{\mathrm{m}}}d_{\mathrm{m}k}}{c}\right)^{\eta}, \text{LoS link}\\ \mathcal{L}_{\mathrm{m}k}^{\mathrm{NLoS}} = \Gamma_2\left(\frac{4\pi f_{\dot{\mathrm{m}}}d_{\mathrm{m}k}}{c}\right)^{\eta}, \text{NLoS link}\end{cases} \tag{15}$$

where $f_{\dot{\mathrm{m}}}$ is the mmWave carrier frequency, and $\Gamma_1$ and $\Gamma_2$ represent the mean values of excessive PL for LoS and NLoS scenarios, respectively. The impact of small-scale fading on the mmWave AtG channels is neglected [56]. Then, the average PL could be expressed as [56]

$$\bar{\mathcal{L}}_{\mathrm{m}k} = P_{\mathrm{m}k}^{\mathrm{LoS}}(\theta_k)\cdot\mathcal{L}_{\mathrm{m}k}^{\mathrm{LoS}} + \big[1-P_{\mathrm{m}k}^{\mathrm{LoS}}(\theta_k)\big]\cdot\mathcal{L}_{\mathrm{m}k}^{\mathrm{NLoS}}. \tag{16}$$

The aerial position of the UAV aerial BS is a function of its antenna beamwidth $\Lambda_{\mathrm{m}}$ in degree, the coverage radius $r_{\mathrm{m}}$, and the height $h_{\mathrm{m}}$. We adopt a commonly used simplified antenna pattern that assumes flat[1] gains in the mainlobe and sidelobe, respectively. The simplified beam pattern of a directional beamforming antenna array is approximately represented as [25]

$$G_t \triangleq G_t(\phi_{\mathrm{a}},\phi_{\mathrm{e}}) = \begin{cases}\frac{G_0}{(\Lambda_{\mathrm{m}}/2)^2}, \phi_{\mathrm{a}}\in[0,2\pi), |\phi_{\mathrm{e}}|\le\frac{\Lambda_{\mathrm{m}}}{2},\\ g_0, \text{otherwise.},\end{cases} \tag{17}$$

where $\phi_{\mathrm{a}}$ and $\phi_{\mathrm{e}}$ are the azimuth and elevation angles of direction. The directional gain of the main lobe is $\frac{G_0}{(\Lambda_{\mathrm{m}}/2)^2}$ with $G_0 = 7500$. In practice, the antenna power gain $g_0$ is considered insignificant outside the main-lobe. Thus, the projection of the main-lobe on the ground is a disc of radius $r_{\mathrm{m}} = h_{\mathrm{m}}\tan(\Lambda_{\mathrm{m}}/2)$. That is, the coverage cell of the UAV is the projection disc of the main lobe due to the huge gap between the main lobe level and the side lobe level [25].

It is assumed that the Doppler effect caused by the UAV's motion is completely adjusted at all user terminals. Consequently, the achievable rate at the $k$th user in the access link (downlink) with UAV aerial BS transmit power $\zeta_{\mathrm{m}}^{\mathrm{T}}$ can be expressed as

$$\hat{\Phi}_{\mathrm{m}k} = \frac{W_{\mathrm{m}}}{K_{\mathrm{m}}}\log_2\left(1+\frac{\zeta_{\mathrm{m}}^{\mathrm{T}}G_tG_r/\bar{\mathcal{L}}_{\mathrm{m}k}}{N_{0,\mathrm{m}}}\right), \tag{18}$$

where $W_{\mathrm{m}}$ is the total mmWave bandwidth, $G_t$ and $G_r$ are the transmit and receive antenna gains, respectively, $K_{\mathrm{m}}$ is the number of users covered by the UAV's footprint, and $N_{0,\mathrm{m}}$ indicates the thermal noise power for the mmWave case. Note that $\frac{W_{\mathrm{m}}}{K_{\mathrm{m}}}$ indicates that an equal bandwidth allocation policy is adopted in this paper. However, an unreliable backhaul can limit the user data rate and also incur delays. The rate constraint directly impacts the network throughput,

[1]This assumption is particularly suitable for a single-cell system wherein sidelobes cause no interference to neighboring cells [57], since the UAV causes no interference to GBS coverage, which operates on sub-6 GHz, this assumption is well justified for the proposed system model.

whereas the delay constraint is critical for control signalling deadlines [58]. In this paper, we only consider the backhaul rate limitation, which is caused by the weather attenuation. As a result, when the total access link throughput exceeds the FSO backhaul capacity at any position during the UAV's circular trajectory, the user rate in (18) cannot be guaranteed. To this end, the effective throughput of the $k$th user associated with the UAV aerial BS could be expressed as

$$\Phi_{\mathrm{m}k} = \begin{cases} \hat{\Phi}_{\mathrm{m}k} & \text{if} \quad \sum_{k=1}^{K_{\mathrm{m}}} \hat{\Phi}_{\mathrm{m}k} \leq \overline{C}_{\mathcal{T}} \\ \dfrac{\hat{\Phi}_{\mathrm{m}k}\overline{C}_{\mathcal{T}}}{\sum_{k=1}^{K_{\mathrm{m}}} \hat{\Phi}_{\mathrm{m}k}} & \text{if} \quad \sum_{k=1}^{K_{\mathrm{m}}} \hat{\Phi}_{\mathrm{m}k} > \overline{C}_{\mathcal{T}}. \end{cases} \tag{19}$$

One typical method is to divide the overall trajectory time $T$ into $N$ different time slots, with the assumption that the UAV's position remains approximately constant within each time slot [18]. To this end, the average sum-throughput of UAV over a complete circular trajectory could be expressed as

$$\bar{\Phi}_{\mathrm{UAV}} = \frac{1}{N}\sum_{n=1}^{N}\sum_{k=1}^{K_{\mathrm{m},n}} \Phi_{\mathrm{m}k}(k,n), \tag{20}$$

where $K_{\mathrm{m},n}$ is the number of users covered by the UAV and $\Phi_{\mathrm{m}k}(k,n)$ is the $k$th user's throughput in the $n$th time slot during its trajectory. It is worth mentioning that to estimate the UAV's average throughput in (20) by covering all possible users under the footprint throughout the circular motion, $N$ should be large enough to minimize location change within each time slot.

### C. GBS-USER COMMUNICATION

Unlike the UAV-to-user wireless channel, the GBS-to-user channels are dominated by the NLoS component, To this end, the PL expression could be stated as [59]

$$\bar{\mathcal{L}}_{\mathrm{s}k} = \Gamma_2 \left(\frac{4\pi f_c d_{\mathrm{s}k}}{c}\right)^{\eta}, \tag{21}$$

where $f_c$ denotes the carrier frequency for the sub-6 GHz transmission, and $d_{\mathrm{s}k} = \sqrt{(x_{\mathrm{s}}-x_k)^2 + (y_{\mathrm{s}}-y_k)^2 + h_{\mathrm{s}}^2}$ is the GBS to user distance with GBS altitude $h_{\mathrm{s}}$. To this end, the data rate of the $k$th user with GBS load $K$ (all users) and a system bandwidth $W_{\mathrm{s}}$ can be expressed as

$$\Phi_{\mathrm{s}k} = \frac{W_{\mathrm{s}}}{K}\log_2\left(1 + \frac{\zeta_{\mathrm{s}}^{\mathrm{T}}/\bar{\mathcal{L}}_{\mathrm{s}k}}{N_{0,\mathrm{s}}}\right), \tag{22}$$

where $\zeta_{\mathrm{s}}^{\mathrm{T}}$ is the transmission power of the GBS and $N_{0,\mathrm{s}}$ indicates the thermal noise power for the sub-6 GHz case. Note that the GBS-user association does not change as the UAV completes its trajectory. That is, the dual-mode nature of the networks permits the GBS to serve all the users where the UAV serves a portion of the users during the UAV's trajectory. To this end, during the UAV's trajectory of $N$ equivalent time slots, the GBS's average throughput could be calculated as follows

$$\bar{\Phi}_{\mathrm{GBS}} = \frac{1}{N}\sum_{n=1}^{N}\sum_{k=1}^{K}\Phi_{\mathrm{s}k}. \tag{23}$$

Note that GBS's sum throughput over $N$ time slots does not change, i.e., $\bar{\Phi}_{\mathrm{GBS}} = \sum_{k=1}^{K}\Phi_{\mathrm{s}k}$. However, the average over $N$ time slots in (23) is used to make the system consistent with the UAV trajectory, and it could also take into account the impact of any change in the channel conditions, e.g., the impact of small-scale fading, user mobility, etc., which are not considered in this paper.

### D. FAIRNESS PERFORMANCE METRIC

Fairness plays a vital role in the user experience and performance of wireless networks. Overall, fairness in wireless networks is about striking a balance between providing a good user experience to all users and efficiently utilizing the limited network resources. Without a fairness metric, the proposed UAV trajectory can offer significant rate disparities among network users. To this end, we employ Jain's fairness index (JFI), which is an important measure of fairness, and it is defined as [60], [61]

$$\Im = \frac{\left(\sum_{k=1}^{K}\bar{\Phi}_k\right)^2}{K\sum_{k=1}^{K}\bar{\Phi}_k^2}, \tag{24}$$

where $\bar{\Phi}_k = \frac{1}{N}\sum_{n=1}^{N}\Phi_k$ represents the average data rate of the $k$th user after a complete UAV circular trajectory, i.e., $\bar{\Phi}_k$ accounts for the average data rate for the $k$th user served by the GBS or the $k$th user jointly served by the GBS and the UAV aerial BS. In comparison to other measures, Jain's index has a fairness criterion that considers all system users, not only the users that are allocated minimal resources. Note that $\Im$ lies in the range $[\frac{1}{K}, 1]$, where $\Im = 1$ corresponds to the fairest allocation, i.e., every user ideally receives the same data rate.

## III. PROBLEM FORMULATION AND RESOURCE ALLOCATION

Note that we derived an average FSO backhaul capacity expression in (13) because it is very complex for a mobile UAV to simultaneously deal with instantaneous backhaul and access link capacities. As a result, an on-board UAV data buffer is assumed to compensate for any mismatch in the data rate of the backhaul and access links. One can also note that both achievable backhaul and access data rates are a function of the UAV's position and trajectory, both of which depend on the UAV's coverage radius $r_{\mathrm{m}}$ and directional antenna beamwidth $\Lambda_{\mathrm{m}}$ for the considered system model.[2]

[2]It is worth noting that additional factors (e.g., the UAV's speed and buffering mechanism) also impact the end-to-end throughput; however, these are assumed to be ideal and could be considered in a future study.

### A. PROBLEM FORMULATION

Given that the horizontal coordinates of the users are known, our objective is to maximize the end-to-end average network throughput, under certain degree of fairness and FSO backhaul capacity constraints, by jointly optimizing the UAV's coverage radius and directional antenna beamwidth, which essentially optimizes the UAV aerial BS's trajectory. Note that the UAV's altitude $h_{\mathrm{m}}$ is a function of both antenna beamwidth $\Lambda_{\mathrm{m}}$ and coverage radius $r_{\mathrm{m}}$, i.e., $h_{\mathrm{m}} = r_{\mathrm{m}} \cot(\Lambda_{\mathrm{m}}/2)$, and $r_{\mathrm{m}}$ is related to the trajectory radius $R_o$ as $r_{\mathrm{m}} = R - R_o$. One can note that the introduction of UAV-enabled mmWave access links for capacity enhancement may result in a massive disparity in the average achievable data rates of users if the trajectory is not properly designed. To handle this, a minimum JFI threshold $\Im_{\mathrm{th}}$ that is commonly used in the studies (e.g., [63]) could be introduced. To this end, the following optimization problem is formulated to enhance the total capacity of the network as

$$(\mathrm{P0}): \max_{r_{\mathrm{m}}, \Lambda_{\mathrm{m}}} \ \bar{\Phi}_{\mathrm{UAV}}(r_{\mathrm{m}}, \Lambda_{\mathrm{m}}) + \bar{\Phi}_{\mathrm{GBS}} \tag{25}$$

$$\text{s.t.} \ \ \bar{\Phi}_{\mathrm{UAV}}(r_{\mathrm{m}}, \Lambda_{\mathrm{m}}) \leq \overline{C}_{\mathcal{T}}, \tag{26}$$

$$\Im_{\mathcal{T}} \geq \Im_{\mathrm{th}}, \tag{27}$$

$$\Lambda_{\min} \leq \Lambda_{\mathrm{m}} \leq \Lambda_{\max}, \tag{28}$$

$$r_{\min} \leq r_{\mathrm{m}} \leq r_{\max}, \tag{29}$$

where constraint (26) denotes that the UAV's mmWave access link throughput cannot exceed its average FSO backhaul capacity, it is ensured to be satisfied by using (19). The constraint in (27) ensures that the system fairness $\Im_{\mathcal{T}}$ is at least $\Im_{\mathrm{th}}$. Constraints in (28) and (29) define the operational limits of the UAV's coverage radius $r_{\mathrm{m}}$ and antenna beamwidth $\Lambda_{\mathrm{m}}$, respectively. In essence, the sum rate of the GBS remains unaffected by changes in the UAV's user association due to the dual-mode operation of users, as the GBS serves all users during the UAV's complete trajectory. Note that the FRMT method considers the fairness constraint in (27) whereas the RMT method ignores the fairness constraint. The performance of the proposed schemes is compared with the benchmark GBS only (GBSO) scheme, i.e., without a UAV deployment.

Note that for a given coverage trajectory based on radius $r_{\mathrm{m}}$ and beamwidth $\Lambda_{\mathrm{m}}$ and FSO gateway location, the UAV's backhaul capacity can be explicitly calculated using (13). However, P0 is non-convex due to the non-concave objective function and the non-convex constraint (27) [64]. In general, there is no systematically efficient method for obtaining the optimal solution. To efficiently handle the trajectory optimization, we employ WOA, a powerful metaheuristic tool that is particularly suitable for UAV trajectory-based scenarios [65]. The application of WOA has been specifically proposed for UAV location, placement, and trajectory optimization problems [66]. In comparison to other heuristic methods, WOA enhances the likelihood of avoiding local optimum solutions. Due to its simple, adaptable, and efficient method, WOA has been employed for a wide variety of network optimization problems in wireless networks [67], [68], [69], [70]. As detailed in [71], it also has a wide spectrum of applications in various engineering domains. Further, as demonstrated in [72], [73], WOA can solve the optimization problems more efficiently in terms of solution quality and convergence speed than the widely used algorithms such as particle swarm optimization (PSO), genetic algorithm (GA), grey wolf optimization (GWO), etc.

### B. WHALE OPTIMIZATION BASED UAV-TRAJECTORY

WOA is a meta-heuristic algorithm inspired by the prey-hunting method of whales. The WOA employs adaptive mechanisms that balance the exploration and exploitation characteristics of the algorithm. In WOA, whale population $\mathsf{X}_i$, $i = \{1, \ldots, \mathsf{N}\}$ is initialized. Each element of this population represents a pair of $r_{\mathrm{m}}$ and $\Lambda_{\mathrm{m}}$ values in the context of our problem. The algorithm determines the position of the best whale $\mathsf{X}^*$, which represents an optimal pair of $r_{\mathrm{m}}^{opt}$ and $\Lambda_{\mathrm{m}}^{opt}$ values (both of which determine the UAV aerial BS's trajectory in Fig. 1) with the aim to maximize the objective (fitness) function of P0 in (25). Note that a minimization objective can be transformed into a maximizing problem in the WOA by adding a negative sign to the objective function. In order to achieve the final goal, the whales' behavior is divided into three main steps [65], [72].

#### 1) ENCIRCLING PREY

When the whales execute this action, before totally engulfing their prey, they first evaluate the position of the prey. The current best whale position is assumed to be quite close to the optimal solution. The position of the other whales is updated based on the best whale's position. The following equations can describe the behavior [65], [72]

$$\vec{\mathsf{D}} = \left| \vec{\mathsf{C}} \cdot \overrightarrow{\mathsf{X}^*}(q) - \vec{\mathsf{X}}(q) \right|, \tag{30}$$

$$\vec{\mathsf{X}}(q+1) = \overrightarrow{\mathsf{X}^*}(q) - \vec{\mathsf{A}} \cdot \vec{\mathsf{D}}, \tag{31}$$

where $\overrightarrow{\mathsf{X}^*}$ denotes the position vector (i.e., $r_{\mathrm{m}}$, $\Lambda_{\mathrm{m}}$) of the best solution (so far) and $\overrightarrow{\mathsf{X}}$ represents the position vector, $q$ is the current iteration, $|.|$ is the absolute value, and '.' denotes the element-wise multiplication. Note that the coefficient vectors $\vec{\mathsf{A}}$ and $\vec{\mathsf{C}}$ are determined as follows

$$\vec{\mathsf{A}} = 2\vec{\mathsf{a}}.\vec{r} - \vec{\mathsf{a}}, \tag{32}$$

$$\vec{\mathsf{C}} = 2.\vec{r}, \tag{33}$$

where $\vec{\mathsf{a}}$ is linearly reduced (2 to 0) over iterations, and $\vec{\mathsf{r}}$ is a random vector in the range [0, 1]. Note that the main purpose of (32) and (33) is to balance the exploration and exploitation for the algorithm.

#### 2) BUBBLE-NET ATTACK METHOD

The spiral equation between the location of the prey and the whale can be used to replicate the helix-shaped movement of humpback whales as follows [65], [72]

$$\vec{\mathsf{D}}' = \left| \overrightarrow{\mathsf{X}^*}(q) - \vec{\mathsf{X}}(q) \right|, \tag{34}$$

$$\vec{\mathsf{X}}(q+1) = \overrightarrow{\mathsf{D}'} \cdot e^{\mathsf{b}\kappa} \cdot \cos(2\pi\kappa) + \overrightarrow{\mathsf{X}^*}(q), \tag{35}$$

where $\mathsf{b}$ denotes the constant value used to determine the logarithmic spiral's shape, and $\kappa$ is a random number in the range $[-1, 1]$.

Since humpback whales swim around their prey in a shrinking circle while also moving along a spiral-shaped course, the shrinking encircling method and the spiral approach are utilized in combination. To model this behavior, it is assumed that each mechanism occurs with a 50% probability, as follows

$$\vec{\mathsf{X}}(q+1) = \begin{cases} \overrightarrow{\mathsf{X}^*}(q) - \vec{\mathsf{A}} \cdot \vec{\mathsf{D}}, & \text{if } \mathsf{p} < 0.5 \\ \overrightarrow{\mathsf{D}'} \cdot e^{\mathsf{b}\kappa} \cdot \cos(2\pi\kappa) + \overrightarrow{\mathsf{X}^*}(q), & \text{if } \mathsf{p} \geq 0.5 \end{cases} \tag{36}$$

where $\mathsf{p}$ is a random in [0, 1].

### 3) SEARCH FOR PREY

Searching for prey (exploration) can be done using the same method based on the variation of the $\vec{A}$ vector. Humpback whales, in fact, search at random based on their location. To push the search agent away from a reference whale, $\vec{A}$ with random values higher than 1 or less than -1 is employed. In the exploration phase, as opposed to the exploitation phase, the position of a search agent is updated based on a randomly selected search agent as opposed to the finest search agent discovered so far. This mechanism and $|\vec{A}| > 1$ emphasize exploration and allow WOA to perform a global search. The mathematical model for prey search is represented as follows [65], [72]

$$\vec{\mathsf{D}} = \left| \vec{\mathsf{C}} \cdot \overrightarrow{\mathsf{X}_{\text{rand}}} - \vec{\mathsf{X}}(q) \right|, \tag{37}$$

$$\vec{\mathsf{X}}(q+1) = \overrightarrow{\mathsf{X}_{\text{rand}}} - \vec{\mathsf{A}} \cdot \vec{\mathsf{D}}, \tag{38}$$

where $\overrightarrow{\mathsf{X}_{\text{rand}}}$ denotes a randomly chosen position vector from the existing population. Note that meta-heuristic algorithms have two phases: exploitation and exploration, which are the bubble-net attacking mechanism and search for prey, respectively. The bubble-net attack strategy exploits the best local solution, while the prey search increases solution diversity for global solutions. Exploitation is preferred in early iterations, but exploration is preferred as iterations increase.

### 4) CONSTRAINT HANDLING

Note that the original WOA was developed for unconstrained optimization problems [65]. To solve the proposed constrained problem, we must use an efficient constraint-handling method. The death penalty [74] is the modest one that constructs the main objective value of the mathematical model to be processed, and the infeasible solutions can be discarded automatically by the heuristic algorithms. Therefore, the death penalty method is employed in this work to tackle the constraint in (27).

Algorithm 1 summarizes the steps of WOA to solve the problem P0. Additional information, such as a more detailed discussion of WOA's working principles and complexity, can be found in [65], [72].

**Algorithm 1:** Optimal UAV Trajectory Using WOA

**Initialize**;
Initialize the whale population $\mathsf{X}_i$, $i = \{1, \ldots, \mathsf{N}\}$, Iteration $q = 1$, maximum number of iterations $\mathsf{I}_{\max}$, Determine the fitness of the search agents and discover the best search agent $\overrightarrow{\mathsf{X}^*}(q)$.
**while** $q < \mathsf{I}_{\max}$ **do**
  **for** $k \leftarrow 1$ *to* $\mathsf{N}$ **do**
    Update $\mathsf{a}, \mathsf{A}, \mathsf{C}, \kappa, \mathsf{p}$.
    **if** $\mathsf{p} < 0.5$ **then**
      **if** $|\mathsf{A}| < 1$ **then**
        Update $\overrightarrow{\mathsf{D}}$ by (30) and $\overrightarrow{\mathsf{X}}$ by (31)
      **else**
        Select a random $\overrightarrow{\mathsf{X}}_{\text{rand}}$ and update $\overrightarrow{\mathsf{D}}$ by (37) Update the position $\overrightarrow{\mathsf{X}}$ by (38)
      **end**
    **else**
      Update $\overrightarrow{\mathsf{D}}$ by (34) and $\overrightarrow{\mathsf{X}}$ by (35)
    **end**
  **end**
  Calculate the fitness of each search agent Update $\mathsf{X}^*(q)$ of the best search agent Increment the index $q = q + 1$.
**end**
Return $\mathsf{X}^*$ (i.e., $r_m^{\text{opt}}$, $\Lambda_m^{\text{opt}}$).

**TABLE 2.** Simulation parameters.

| FSO Link [4], [7] | | |
|---|---|---|
| Parameter | Symbol | Value |
| FSO wavelength | $\lambda_o$ | 1550 nm |
| Receiver diameter | $\gamma$ | 5 cm |
| Beam divergence | $\phi$ | 2.5 mrad |
| Responsivity | $\rho$ | $0.7V^{-1}$ |
| Noise variance | $\sigma_o^2$ | $10^{-14}A^2$ |
| Transmit power | $\zeta_o$ | 50 mW |
| Bandwidth | $W_o$ | 1 GHz |
| RF Link [25], [62] | | |
| Parameter | Symbol | Value |
| Carrier Frequency | $f_c, f_{\text{m}}$ | 2, 28 GHz |
| Bandwidth | $W_{\text{s}}, W_{\text{m}}$ | 30, 300 MHz |
| GBS transmit power | $\zeta_{\text{s}}^{\text{T}}$ | 35 dBm |
| UAV transmit power | $\zeta_{\text{m}}^{\text{T}}$ | 32 dBm |
| Additional path loss LoS, NLoS | $\Gamma_1, \Gamma_2$ | 3 dB, 23 dB |
| Environment parameter | $\omega_1, \omega_2$ | 12.08, 0.11 |
| Noise power | $N_{0,\text{m}}, N_{0,\text{s}}$ | -96 dBm, -99 dBm |

## IV. RESULTS AND SYSTEM PERFORMANCE

In this section, simulation results demonstrating the performance of the proposed trajectory optimization model depicted in Fig. 1 are presented. Unless otherwise stated, the values of the system parameters used for the numerical simulations are listed in Table 2. The WOA parameters are population size $\mathsf{N}$ =150 and total iterations $\mathsf{I}_{\max}$ =500. The

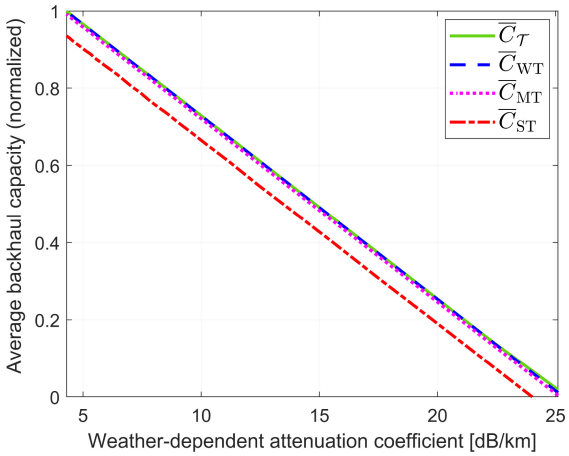


**FIGURE 3.** Average FSO backhaul capacity (normalized) for the proposed scheme, and under conditions of weak, moderate, and strong atmospheric turbulence using $\Lambda_{\max} = 120^{\circ}$ and $r_{\mathrm{m}} = 100$ m.

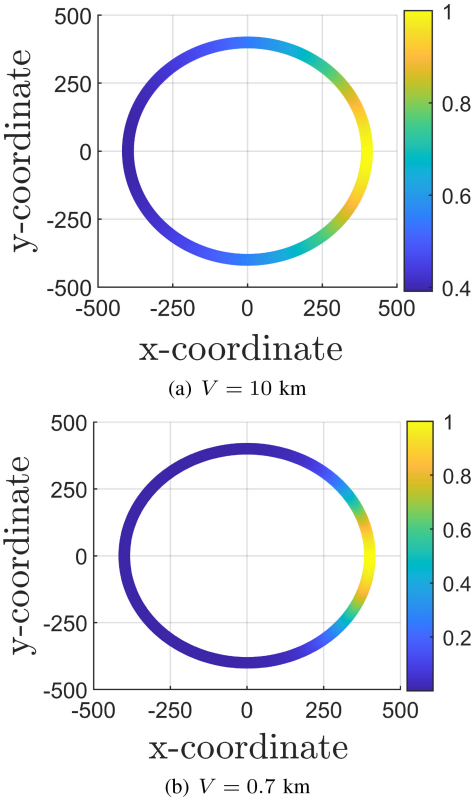


**FIGURE 4.** The FSO channel capacity (normalized) variations at different UAV positions ($N = 360$) during its circular trajectory under two different visibility $V$ conditions using $\Lambda_{\max} = 120^{\circ}$ and $r_{\mathrm{m}} = 100$ m.

FSO gateway $\mathcal{G}$ is located $d_{\mathcal{G}} = 800$ meters away from the origin of the coverage area. Note that the wavelength of 1550 nm is preferred for FSO transmissions over alternatives like 850 nm, 1300 nm, and 1064 nm due to its advantages in eye safety, compatibility with current and future all-optical networks, and its ability to transmit significantly higher laser power with safe operation [75]. Also, the operational range of beamwidth $\Lambda_{\mathrm{m}} \in [\Lambda_{\min}, \Lambda_{\max}]$ is adopted as given in [76]. The minimum UAV coverage radius is $r_{\min} = 50$ m, and by design, $r_{\max} = R/2$. Also, a unity receiver antenna gain ($G_r = 1$) is considered in this paper. The fifth-percentile throughput, which 5G explicitly identifies as a key performance metric [77], is a performance indicator and represents the throughput attained by a specimen of worst-case users [78]. The fifth-percentile throughput increases with an increase in JFI, i.e., a higher fairness index suggests a more even distribution of resources, so even the network's lowest-performing users are likely to receive a higher minimum level of service.

Firstly, we incorporate the influence of atmospheric turbulence into the average backhaul channel capacity in Fig. 3. This is achieved through $5 \times 10^3$ Monte Carlo trials, considering weak, moderate, and strong turbulence scenarios with corresponding refraction structure parameter $C_n^2$ of $1 \times 10^{-15}$ m$^{-2/3}$, $1 \times 10^{-14}$ m$^{-2/3}$, and $1 \times 10^{-13}$ m$^{-2/3}$ [42], respectively. It can be observed that the results for the proposed average backhaul capacity $\overline{C}_{\mathcal{T}}$ presented in (13), which is derived under turbulence-free conditions, are comparable to the average channel capacity under weak and moderate turbulence conditions, denoted as $\overline{C}_{\mathrm{WT}}$ and $\overline{C}_{\mathrm{MT}}$, respectively. This is due to the circular trajectory's averaging effect; that is, as the UAV moves along the circular trajectory, rapid fluctuations due to turbulence-induced intensity fluctuations occur; however, due to the average capacity over the entire trajectory, these rapid fluctuations are effectively mitigated under weak and moderate turbulence, rendering the overall turbulence effects negligible. Moreover, due to the higher altitude of the UAV link and the foggy conditions, turbulence tends to be weak or moderate, for which a very close match exists. However, under strong turbulence conditions, a substantial channel capacity attenuation is encountered, which degrades the average backhaul capacity $\overline{C}_{\mathrm{ST}}$. Thus, one could conclude that the proposed trajectory-based design is well suited for low and moderate turbulence regimes. Note that since this work focuses on system performance during fog events, it is reasonable to assume weak to moderate turbulence conditions, owing to the inverse relationship between the foggy condition and the strength of atmospheric turbulence.

In Fig. 4, we illustrate the FSO channel capacity (normalized) along a UAV's circular trajectory comprising $N = 360$ equidistant points, considering low and high visibility conditions. It is evident that significant capacity variations arise due to the UAV's changing position relative to the FSO gateway, persisting across both low and high visibility conditions. Notably, under low visibility ($V = 0.7$ km), heightened variations occur due to increased attenuation. These findings underscore challenges in managing backhaul and access capacities simultaneously and suggest user fairness concerns across positions. Hence, all subsequent results are based on the average FSO backhaul channel capacity given in (13) for the entire trajectory. Note that it is important to realize the impact of weather attenuation

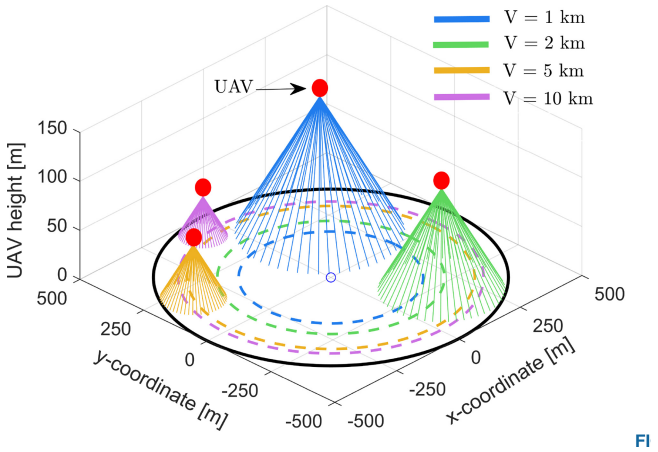


FIGURE 5. An illustrative snapshot of the UAV's circular trajectory and coverage radius for backhaul capacity maximization design under four visibility conditions.

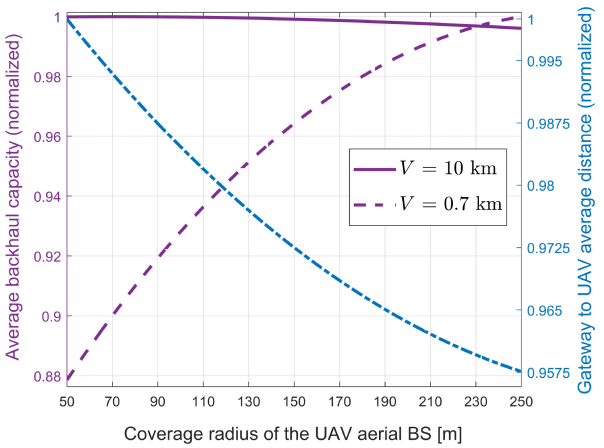


FIGURE 6. Average FSO backhaul capacity (normalized) under both high and low visibility conditions, and the normalized average distance between the FSO gateway and UAV for varying UAV coverage radii, $r_m$.

on the trajectory of the UAV aerial BS when only the FSO backhaul link is taken into account.

The results in Fig. 5 plot one illustrative snapshot of the UAV's positioning during its trajectory to show the impact of visibility conditions on the positioning of the UAV when the mmWave access link is disregarded, i.e., a UAV trajectory with an optimal FSO backhaul capacity is selected. One can clearly see that during good weather conditions (e.g., $V = 10$ km), the UAV tends to fly at the cell edge. However, as the visibility decreases (weather attenuation increases), the UAV changes its trajectory and flies closer to the origin of the GBS's coverage area. Note that this plot only deals with the change in the UAV's position for an optimal backhaul capacity under different visibility conditions; however, the UAV's footprint on the ground is depicted to reveal the reflection of its changing position on its coverage area under the employed model. Since the backhaul capacity could be a driving force for the UAV's positioning, it is important to discern this shift in the UAV's positioning before moving on to the results that include the access link of the UAV aerial BS for end-to-end system throughput.

Fig. 6 plots the average FSO backhaul capacity (normalized) and average distance (normalized) between FSO gateway $\mathcal{G}$ and UAV for different UAV coverage radii. Note that the average backhaul capacities in this plot have been normalized using the maximum value within each visibility condition to clearly depict how the average channel capacity changes with the UAV position. Otherwise, as expected, high-visibility scenarios have a substantially greater average backhaul capacity.

One can note that the average distance gradually decreases as the UAV moves closer to the origin. However, despite a slightly higher average distance, the UAV prefers to fly close to the cell edge during high visibility conditions ($V = 10$ km), i.e., the UAV's average backhaul capacity is highest when it flies closer to the edge. It is critical to highlight that the change in FSO backhaul capacity along the trajectory of the UAV is non-linear due to the non-linearly varying distance. This non-linearity introduces backhaul capacity variations at different positions. For instance, the UAV's backhaul capacity is expected to be highest for the UAV's trajectory arc, which is close to the FSO gateway in Fig. 1, with the lowest UAV coverage radius. Whereas the backhaul capacity is expected to be lowest for the arc of the trajectory, which is located on the other side of the coverage area, opposite to the FSO gateway. However, as shown in Fig. 6, the average backhaul capacity sees a minimal change as the UAV coverage radius is changed from a low to a high value in good visibility conditions. Conversely, under low visibility ($V = 0.7$ km), the opposite happens: the UAV shifts its trajectory closer to the origin of the cell. That is, the average backhaul capacity witnesses an increase as the UAV coverage radius $r_m$ increases in low visibility. This is due to the fact that during an adverse weather situation, a slight increase in distance can cause significant attenuation; hence, the UAV aerial BS tends to fly closer to the origin to minimize the impact of distance-based attenuation. Also, in adverse weather, the trajectory arc on the opposite side of the FSO gateway could produce substantially lower channel capacity (due to an increased distance). This in turn, in adverse weather, dictates the UAV to fly closer to the origin, where the average backhaul capacity is better than in the cell-edge scenario. Whereas during more frequent normal weather conditions, the UAV takes advantage of flying at the cell edge.

Henceforth, the results are presented by solving the problem P0, i.e., the impact of both access and backhaul links is incorporated using the UAV's parameters (coverage radius $r_{\mathrm{m}}$ and antenna beamwidth $\Lambda_{\mathrm{m}}$), which are optimized for an optimal UAV 3D circular trajectory. According to (17), to achieve a high directional antenna gain, a minimal practical value of beamwidth $\Lambda_m$ should be employed. It follows that the UAV is expected to operate with a narrow beamwidth from the viewpoint of the ground users of the UAV aerial BS to harvest more gain. Fig. 7 gives a pictorial account

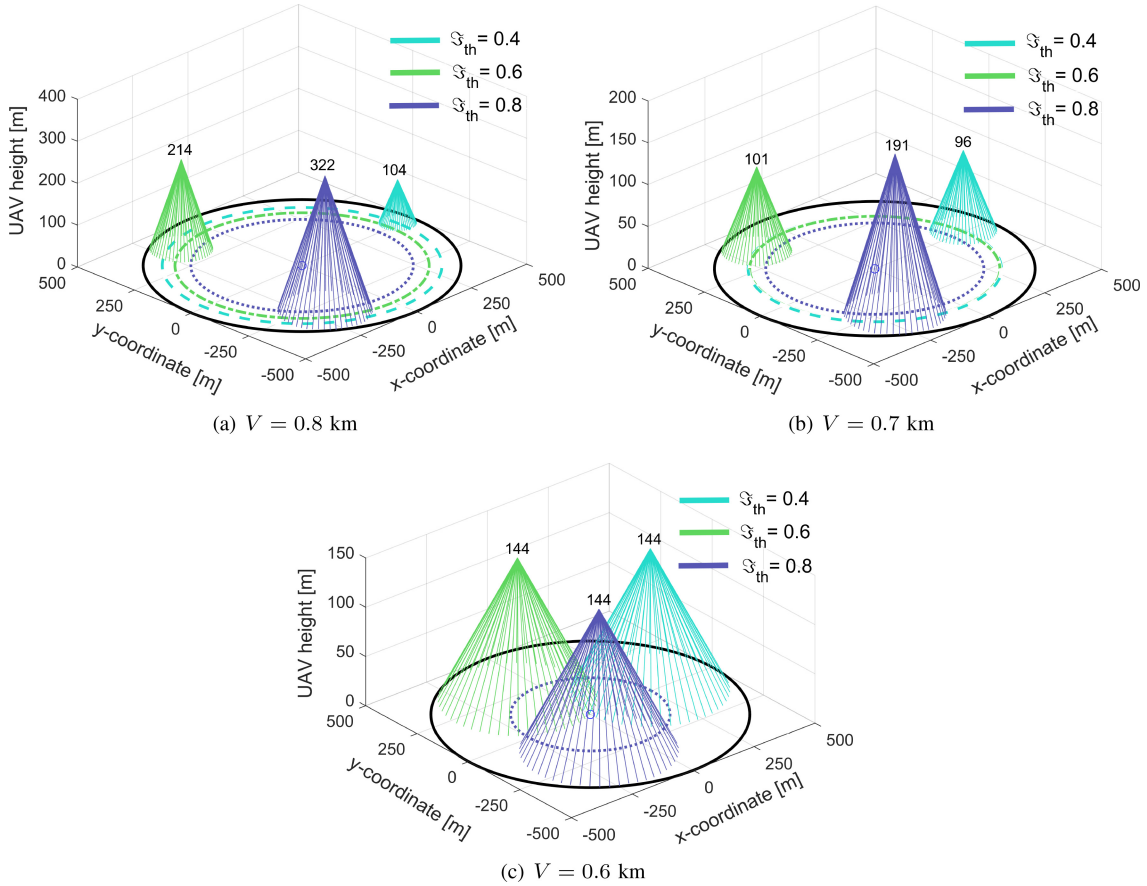


(a) $V = 0.8$ km (b) $V = 0.7$ km

(c) $V = 0.6$ km

**FIGURE 7.** The 3D coverage footprint of the UAV using the FRMT approach under three different thresholds $\Im_{th}$, based on three different weather attenuation conditions.

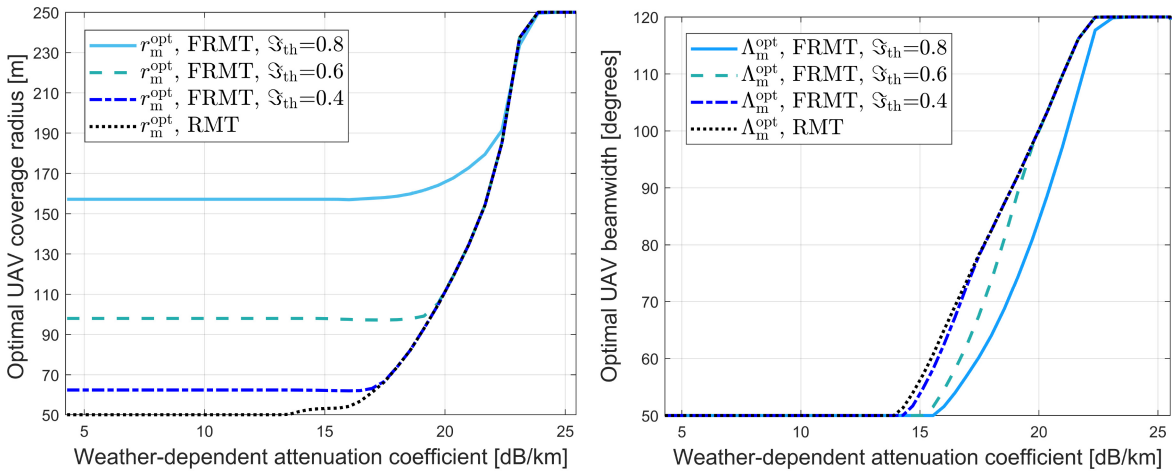


(a) UAV optimal coverage radius, $r_m^{\text{opt}}$ (b) UAV optimal antenna beamwidth, $\Lambda_m^{\text{opt}}$

**FIGURE 8.** Optimal UAV coverage radius and antenna beamwidth versus weather attenuation under three cases of fairness threshold.

of the UAV changing its optimal coverage radius $r_{\text{m}}^{\text{opt}}$ (and beamwidth $\Lambda_{\text{m}}^{\text{opt}}$) for three fairness threshold $\Im_{\text{th}}$ values under three low visibility conditions using the FRMT method. As expected, UAV covers more area as the fairness threshold $\Im_{\text{th}}$ is increased. It is also worth noting that the UAV's coverage radius increases as the visibility decreases; this is because the UAV's backhaul is compromised by the adverse weather and it tends to fly closer to the origin, unlike during normal weather conditions. Also note that, from the access link's viewpoint, the UAV increases its coverage radius due to the nature of the disc-based model. That is, when the UAV flies closer to its origin, it covers more area.

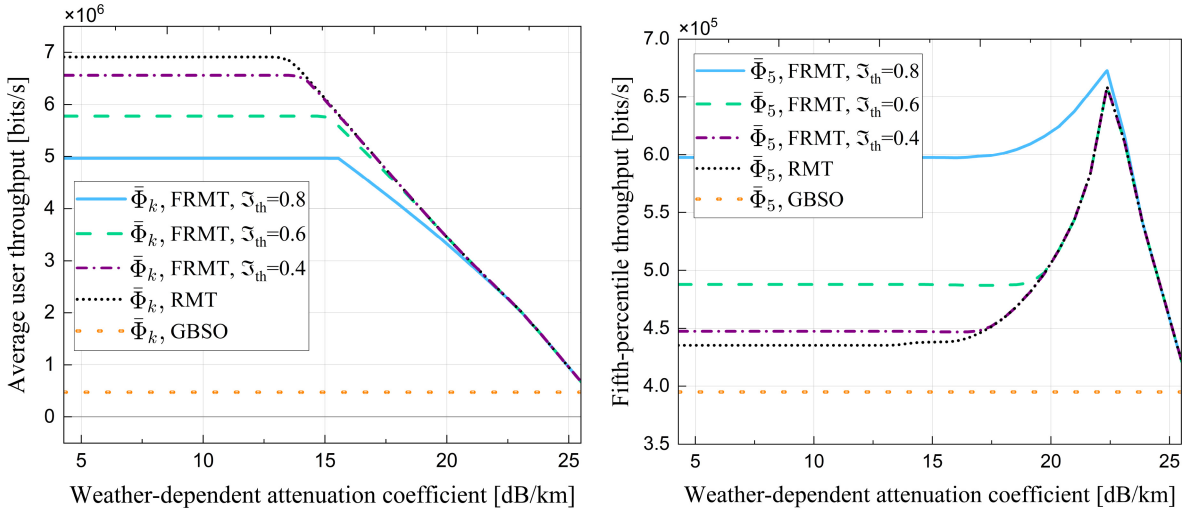


(a) Average user throughput [bits/s] (b) Fifth-percentile throughput [bits/s]

**FIGURE 9.** Average user throughput and fifth-percentile throughput of the network under three cases of fairness threshold $\Im_{th}$.

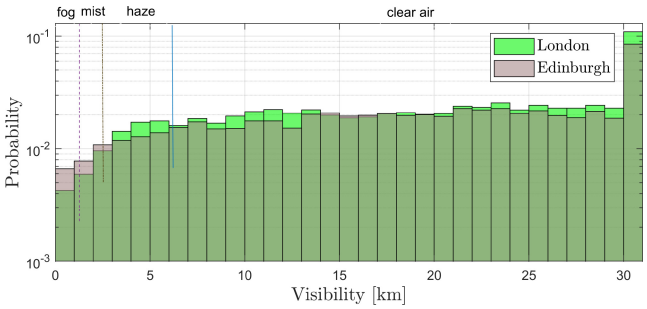


**FIGURE 10.** Hourly visibility histogram for Edinburgh and London from January 2019 to June 2020.

## V. APPLICATION USING PRACTICAL MEASUREMENTS

The results in Fig. 8 show the optimal UAV coverage radius $r_{\mathrm{m}}^{\mathrm{opt}}$ and antenna beamwidth $\Lambda_{\mathrm{m}}^{\mathrm{opt}}$ in Fig. 8(a) and Fig. 8(b), respectively, for FRMT and RMT methods under different weather attenuation conditions. One can note that the FRMT offers more UAV coverage compared to its RMT counterpart, and the UAV's coverage radius increases as the fairness threshold $\Im_{\mathrm{th}}$ is increased. This is due to the fact that higher fairness is achieved when UAV cover more users. Also, an increase in weather attenuation hampers its backhaul capacity; the UAV tends to fly closer to the origin, hence increased UAV coverage, to reduce the impact of weather attenuation. The directional antenna beamwidth also increases because the UAV tends to fly as low as possible to minimize the distance from the gateway $\mathcal{G}$. It is worth mentioning that for the antenna model given in (17), UAV offers a higher gain at low beamwidth values, i.e., $G_0/(\Lambda_{\mathrm{m}}/2)^2$. For this reason, UAV tries to keep a low beamwidth profile to harvest more gain in the access link during low weather attenuation. However, one can note that for a given coverage radius, the UAV needs to fly higher at low beamwidth values, i.e., $h_{\mathrm{m}} = r_{\mathrm{m}} \cot(\Lambda_{\mathrm{m}}/2)$, which indicates that from the access link's viewpoint, cell-edge (low UAV coverage radius) offers a combination of low beamwidth and low height (lower PL), compared to when the UAV is close to the origin. For this reason, when the UAV has a reliable backhaul, it tends to have a lower coverage radius and beamwidth. However, as the weather attenuation increases, its backhaul is compromised, and the UAV shifts closer to the origin as higher values of $r_{\mathrm{m}}^{\mathrm{opt}}$ and $\Lambda_{\mathrm{m}}^{\mathrm{opt}}$ are desirable to fly as low as possible to minimize the impact on its backhaul. In essence, as the visibility diminishes, the concern shifts from extracting the most from the mmWave access link to the FSO backhaul, and the UAV moves closer to the origin, in which, by design, the UAV has a larger coverage footprint.

The optimal average user throughput $\bar{\Phi}_k$ and fifth-percentile throughput $\bar{\Phi}_5$ of the RMT, FRMT, and GBSO systems are plotted in Fig. 9. It is evident that the RMT and FRMT methods outperform the GBSO deployment for both performance metrics during different weather attenuation situations. One can also observe that there is a performance tradeoff between $\bar{\Phi}_k$ and $\bar{\Phi}_5$ metrics for RMT and FRMT methods. That is, as the fairness threshold $\Im_{\mathrm{th}}$ of the FRMT method increases, $\bar{\Phi}_k$ diminishes, but $\bar{\Phi}_5$ tends to improve. It is also worth noticing that the performance of both RMT and FRMT methods converges under higher weather attenuation coefficient $\vartheta$ values. This is due to the fact that for higher weather attenuation, the UAV shifts its trajectory closer to the origin to reduce the adverse impact of weather on its backhaul capacity and reaches its maximum value of $\frac{R}{2}$ radius. The proposed systems enable some capacity gain even at high weather attenuation (e.g., 25 dB/km), which encourages the use of FSO-based backhauling to keep functioning under certain adverse conditions.

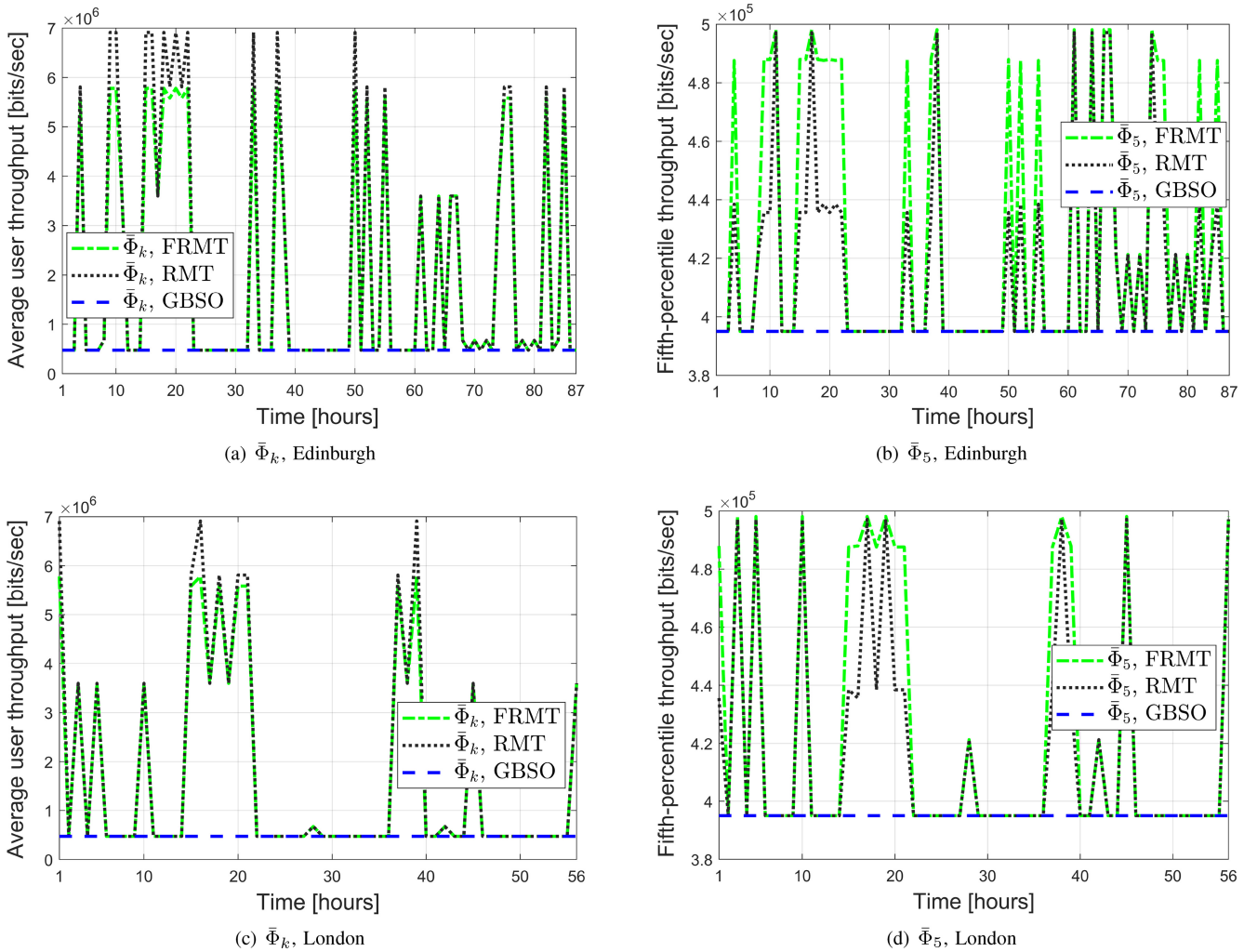


(a) $\bar{\Phi}_k$, Edinburgh

(b) $\bar{\Phi}_5$, Edinburgh

(c) $\bar{\Phi}_k$, London

(d) $\bar{\Phi}_5$, London

**FIGURE 11.** The average achievable user data rate $\bar{\Phi}_k$ and fifth-percentile throughput $\bar{\Phi}_5$ of the users ($\Im_{\text{th}} = 0.6$) versus the fog hours in Edinburgh and London from January 2019 to June 2020.

According to the international definition, fog, mist, and haze are defined as visibility of $V < 1$ km, $1 \leq V < 2$ km, and $2 \leq V < 5$ km, respectively. Fig. 10 plots the histogram of hourly visibility for the cities of Edinburgh and London as reported by the United Kingdom Meteorological Office for January 2019 to June 2020, totaling $\mathsf{H}_{\text{tot}} =$ 13,106 hours (Edinburgh), $\mathsf{H}_{\text{tot}} =$ 13,128 hours (London). As can be seen, the probability of fog events (visibility $<$ 1 km), which can severely deteriorate the FSO link's performance, is significantly small. This indicates that adverse weather conditions, such as fog, are not frequent in many geographical areas. The fact that FSO links operate effectively the majority of the time in typical weather conditions paves the way for the UAV aerial BS to simply play its role in enhancing the capacity of the system. Despite very rare low visibility conditions, however, it is interesting to evaluate the performance of FSO-based systems in these practical conditions.

The cities of Edinburgh and London experienced only 87 and 56 hours of fog events (visibility $<$ 1 km), respectively, from January 2019 to June 2020, which is only almost 0.66% and 0.43% of the specified duration. To this end, FSO-based backhauling is assumed to be very rarely compromised. The performance of the FSO links is always expected to be better in the two other weather attenuation conditions, mist and haze, because fog delivers the worst weather attenuation for the FSO links. To this end, we only investigate the performance of the proposed system using the practical weather data from the cities of Edinburgh and London for the foggy channel conditions, i.e., visibility $<$ 1 km.

Fig. 11 shows the average user data rate $\bar{\Phi}_k$ and fifth-percentile throughput $\bar{\Phi}_5$ in Edinburgh and London for low visibility conditions under the fairness threshold $\Im_{\text{th}} = 0.6$. One can see that even in rare low visibility conditions, the proposed trajectory-based methods RMT and FRMT show significant performance improvements on most occasions using both $\bar{\Phi}_k$ and $\bar{\Phi}_5$ metrics. For example, during fog hours 10 and 16 in Edinburgh and London, respectively, substantial improvement could be witnessed in terms of both average user throughput $\bar{\Phi}_k$ and fifth-percentile throughput

$\bar{\Phi}_5$ compared to the GBSO case. Moreover, as expected, the RMT design performs better than FRMT in terms of $\bar{\Phi}_k$ in Fig. 11(a) and Fig. 11(c), whereas FRMT outperforms its counterpart RMT for the $\bar{\Phi}_5$ metric in Fig. 11(b) and Fig. 11(d). It is also worth pointing out that on some occasions (e.g., dense fog) during low-visibility conditions, the FSO backhaul is totally compromised, as seen during fog hours 30 and 50 in Edinburgh and London, respectively.

One can also visualize that the proposed RMT and FRMT trajectory schemes will offer similar performance with a tradeoff between achievable data rate and fifth-percentile throughput when the system is investigated using other values of the JFI threshold $\Im_{\text{th}}$ (e.g., 0.4, 0.8) using real data. Moreover, it could also be concluded that when the practical data for mist and haze is applied, the proposed RMT and FRMT methods are considered to display much better performance than in low visibility conditions. Hence, the proposed schemes offer substantial capacity enhancement on several occasions, even in rare foggy channel conditions, and the fairness threshold could be adjusted to meet a desired system-level fairness. These findings indicate that UAV-aided FSO backhauling can substantially enhance system performance and capacity not only in more frequent normal weather situations but also in rare adverse weather conditions, e.g., thin, light, and moderately foggy channel conditions.

## VI. CONCLUSION

This paper proposes a UAV-aided network capacity enhancement technique that takes into account the UAV backhaul situation to optimize its circular trajectory for maximizing the end-to-end capacity of the network with a degree of fairness. The UAV aerial BS is considered to be backhauled using an FSO link for the capacity enhancement of a network served by a GBS. We have shown that the UAV adaptively changes its trajectory using the relevant parameters (e.g., coverage radius, antenna beamwidth) owing to the impact of existing weather conditions on the FSO backhaul link. As expected, the UAV's coverage footprint increases with an increase in the fairness requirement. Specifically, during more frequent good weather conditions, the reliability of the backhaul is not a concern as its FSO link offers high capacity and the UAV's coverage varies as the fairness threshold is changed. However, as the weather attenuation increases, the UAV adaptively changes its trajectory to minimize the adverse impact of weather on its backhaul. In other words, as the weather changes from good to bad, the concern shifts from the UAV's access link to its backhaul link, and the UAV alters its trajectory adaptively. Results based on practical weather measurements also reveal that the proposed methods can enhance the capacity of the network in several low-visibility situations. Practical applications of such UAV-aided capacity enhancement could be witnessed during events or high-demand places in future wireless networks. This work could be extended to explore the effects of a circular trajectory with multiple UAVs. Also, the impact of the UAV's velocity on highly directional backhaul links could be a promising direction to pursue.

## ACKNOWLEDGMENT

The authors are grateful to the Meteorological Office of the United Kingdom for supplying measured hourly visibility data for January 2019 to June 2020 from the Edinburgh Gogarbank and the London Heathrow weather stations.

## REFERENCES

[1] M. M. U. Chowdhury, S. J. Maeng, E. Bulut, and S. Güvenç, "3-D trajectory optimization in UAV-assisted cellular networks considering antenna radiation pattern and backhaul constraint," *IEEE Trans. Aerosp. Electron. Syst.*, vol. 56, no. 5, pp. 3735–3750, Oct. 2020.

[2] N. Tafintsev et al., "Aerial access and backhaul in mmWave B5G systems: Performance dynamics and optimization," *IEEE Commun. Mag.*, vol. 58, no. 2, pp. 93–99, Feb. 2020.

[3] J.-H. Lee, K.-H. Park, Y.-C. Ko, and M.-S. Alouini, "spectral-efficient network design for high-altitude platform station networks with mixed RF/FSO systems," *IEEE Trans. Wireless Commun.*, vol. 21, no. 9, pp. 7072–7087, Sep. 2022.

[4] M. T. Dabiri et al., "UAV-assisted free space optical communication system with amplify-and-forward relaying," *IEEE Trans. Veh. Technol.*, vol. 70, no. 9, pp. 8926–8936, Sep. 2021.

[5] M. Najafi, H. Ajam, V. Jamali, P. D. Diamantoulakis, G. K. Karagiannidis, and R. Schober, "Statistical modeling of the FSO fronthaul channel for UAV-based communications," *IEEE Trans. Commun.*, vol. 68, no. 6, pp. 3720–3736, Jun. 2020.

[6] S. Seo, D.-E. Ko, and J.-M. Chung, "Combined time bound optimization of control, communication, and data processing for FSO-based 6G UAV aerial networks," *ETRI J.*, vol. 42, no. 5, pp. 700–711, 2020.

[7] S. Huang, V. Shah-Mansouri, and M. Safari, "Game-theoretic spectrum trading in RF relay-assisted free-space optical communications," *IEEE Trans. Wireless Commun.*, vol. 18, no. 10, pp. 4803–4815, Oct. 2019.

[8] M. Choi, S. Song, D.-E. Ko, and J.-M. Chung, "Trajectory optimization for FSO based U-IoT backhaul networks," *IEEE Trans. Netw. Sci. Eng.*, vol. 10, no. 4, pp. 2030–2044, Jul./Aug. 2023.

[9] A. Upadhya, "Investigation of mixed RF/FSO decode-and-forward NOMA cooperative relaying networks," *Wireless Pers. Commun.*, vol. 124, no. 4, pp. 2923–2938, 2022.

[10] A. Goel and R. Bhatia, "Joint impact of interference and hardware impairments on the performance of mixed RF/FSO cooperative relay networks," *Opt. Quantum Electron.*, vol. 53, no. 9, p. 530, 2021.

[11] W. Jiang, B. Han, M. A. Habibi, and H. D. Schotten, "The road towards 6G: A comprehensive survey," *IEEE Open J. Commun. Soc.*, vol. 2, pp. 334–366, 2021.

[12] X. Liu, Y. Liu, and Y. Chen, "Reinforcement learning in multiple-UAV networks: Deployment and movement design," *IEEE Trans. Veh. Technol.*, vol. 68, no. 8, pp. 8036–8049, Aug. 2019.

[13] S. Zhang and N. Ansari, "3D drone base station placement and resource allocation with FSO-based backhaul in hotspots," *IEEE Trans. Veh. Technol.*, vol. 69, no. 3, pp. 3322–3329, Mar. 2020.

[14] J. Lyu, Y. Zeng, and R. Zhang, "UAV-aided offloading for cellular hotspot," *IEEE Trans. Wireless Commun.*, vol. 17, no. 6, pp. 3988–4001, Jun. 2018.

[15] M. A. Ali and A. Jamalipour, "UAV-aided cellular operation by user offloading," *IEEE Internet Things J.*, vol. 8, no. 12, pp. 9855–9864, Jun. 2021.

[16] T. Gupta, F. Arena, and I. You, "Efficient resource allocation for backhaul-aware unmanned air vehicles-to-everything (U2X)," *Sensors*, vol. 20, no. 10, p. 2994, 2020.

[17] S. Song, M. Choi, D.-E. Ko, and J.-M. Chung, "Multi-UAV trajectory optimization considering collisions in FSO communication networks," *IEEE J. Sel. Areas Commun.*, vol. 39, no. 11, pp. 3378–3394, Nov. 2021.

[18] F. Cheng et al., "UAV trajectory optimization for data offloading at the edge of multiple cells," *IEEE Trans. Veh. Technol.*, vol. 67, no. 7, pp. 6732–6736, Jul. 2018.

[19] N. Tang, H. Tang, B. Li, and X. Yuan, "Joint maneuver and beamwidth optimization for UAV-enabled multicasting," *IEEE Access*, vol. 7, pp. 149503–149514, 2019.

[20] L. Xiao, Y. Liang, C. Weng, D. Yang, and Q. Zhao, "UAV-enabled data collection: Multiple access, trajectory optimization, and energy trade-off," *Wireless Commun. Mobile Comput.*, vol. 2019, no. 1, 2019, Art. no. 9647539.

[21] N. Gupta, S. Agarwal, and D. Mishra, "Trajectory design for throughput maximization in UAV-assisted communication system," *IEEE Trans. Green Commun. Netw.*, vol. 5, no. 3, pp. 1319–1332, Sep. 2021.

[22] M. T. Dabiri and S. M. S. Sadough, "Optimal placement of UAV-assisted free-space optical communication systems with DF relaying," *IEEE Commun. Lett.*, vol. 24, no. 1, pp. 155–158, Jan. 2020.

[23] M. Elamassie and M. Uysal, "FSO-based multi-layer airborne backhaul networks," *IEEE Trans. Veh. Technol.*, early access, May 27, 2024, doi: 10.1109/TVT.2024.3405735.

[24] J.-H. Lee, K.-H. Park, Y.-C. Ko, and M.-S. Alouini, "A UAV-mounted free space optical communication: Trajectory optimization for flight time," *IEEE Trans. Wireless Commun.*, vol. 19, no. 3, pp. 1610–1621, Mar. 2020.

[25] H. Wu, Z. Wei, Y. Hou, N. Zhang, and X. Tao, "Cell-edge user offloading via flying UAV in non-uniform heterogeneous cellular networks," *IEEE Trans. Wireless Commun.*, vol. 19, no. 4, pp. 2411–2426, Apr. 2020.

[26] İ. Baştürk, "Energy-efficient communication for UAV-enabled mobile relay networks," *Comput. Netw.*, vol. 213, Aug. 2022, Art. no. 109071.

[27] D.-E. Ko, S. Song, M. Choi, and J.-M. Chung, "Cloud shape and attenuation based UAV trajectory optimization for FSO communication," *IEEE Trans. Veh. Technol.*, early access, Feb. 6, 2024, doi: 10.1109/TVT.2024.3362952.

[28] D. Tyrovolas et al., "Energy-aware trajectory optimization for UAV-mounted RIS and full-duplex relay," *IEEE Internet Things J.*, vol. 11, no. 13, pp. 24259–24272, Jul. 2024.

[29] D. Schulz et al., "Robust optical wireless link for the backhaul and fronthaul of small radio cells," *J. Lightw. Technol.*, vol. 34, no. 6, pp. 1523–1532, Feb. 11, 2016.

[30] K. Dautov, N. Kalikulov, and R. C. Kizilirmak, "The impact of various weather conditions on vertical FSO links," in *Proc. IEEE 11th Int. Conf. Appl. Inf. Commun. Technol. (AICT)*, 2017, pp. 1–4.

[31] S. Malik and P. K. Sahu, "Free space optics/millimeter-wave based vertical and horizontal terrestrial backhaul network for 5G," *Opt. Commun.*, vol. 459, Mar. 2020, Art. no. 125010.

[32] L. Yu, X. Sun, S. Shao, Y. Chen, and R. Albelaihi, "Backhaul-aware drone base station placement and resource management for FSO-based drone-assisted mobile networks," *IEEE Trans. Netw. Sci. Eng.*, vol. 10, no. 3, pp. 1659–1668, May/Jun. 2023.

[33] M. Cheng, J.-B. Wang, J. Cheng, J.-Y. Wang, and M. Lin, "Joint scheduling and precoding for mmWave and sub-6 GHz dual-mode networks," *IEEE Trans. Veh. Technol.*, vol. 69, no. 11, pp. 13098–13111, Nov. 2020.

[34] S. Islam, M. Zada, and H. Yoo, "Highly compact integrated sub-6 GHz and millimeter-wave band antenna array for 5G smartphone communications," *IEEE Trans. Antennas Propag.*, vol. 70, no. 12, pp. 11629–11638, Dec. 2022.

[35] C. Saha, M. Afshang, and H. S. Dhillon, "Bandwidth partitioning and downlink analysis in millimeter wave integrated access and backhaul for 5G," *IEEE Trans. Wireless Commun.*, vol. 17, no. 12, pp. 8195–8210, Dec. 2018.

[36] H.-B. Chang and I. Rubin, "Optimal downlink and uplink fractional frequency reuse in cellular wireless networks," *IEEE Trans. Veh. Technol.*, vol. 65, no. 4, pp. 2295–2308, Apr. 2016.

[37] Y. Zeng and R. Zhang, "Energy-efficient UAV communication with trajectory optimization," *IEEE Trans. Wireless Commun.*, vol. 16, no. 6, pp. 3747–3760, Jun. 2017.

[38] C. A. Balanis, *Antenna Theory: Analysis and Design*. Hoboken, NJ, USA: Wiley, 2015.

[39] J.-H. Lee, K.-H. Park, Y.-C. Ko, and M.-S. Alouini, "Throughput maximization of mixed FSO/RF UAV-aided mobile relaying with a buffer," *IEEE Trans. Wireless Commun.*, vol. 20, no. 1, pp. 683–694, Jan. 2021.

[40] R. Abdelfatah, N. Alshaer, and T. Ismail, "A review on pointing, acquisition, and tracking approaches in UAV-based FSO communication systems," *Opt. Quantum Electron.*, vol. 54, no. 9, p. 571, 2022.

[41] A. Harris, J. Sluss, H. Refai, and P. LoPresti, "Alignment and tracking of a free-space optical communications link to a UAV," in *Proc. 24th Digit. Avion. Syst. Conf.*, vol. 1, pp. 1.C.2-1–1.C.2-9, 2005.

[42] A. A. Farid and S. Hranilovic, "Outage capacity optimization for free-space optical links with pointing errors," *J. Lightw. Technol.*, vol. 25, no. 7, pp. 1702–1710, Jul. 2007.

[43] M. Grabner and V. Kvicera, "Multiple scattering in rain and fog on free-space optical links," *J. Lightw. Technol.*, vol. 32, no. 3, pp. 513–520, Feb. 1, 2014.

[44] S. Muhammad, P. Kohldorfer, and E. Leitgeb, "Channel modeling for terrestrial free space optical links," in *Proc. 7th Int. Conf. Transp. Opt. Netw.*, vol. 1, 2005, pp. 407–410.

[45] B. B. Yousif, E. E. Elsayed, and M. M. Alzalabani, "Atmospheric turbulence mitigation using spatial mode multiplexing and modified pulse position modulation in hybrid RF/FSO orbital-angular-momentum multiplexed based on MIMO wireless communications system," *Opt. Commun.*, vol. 436, pp. 197–208, Apr. 2019.

[46] R. Bosu and S. Prince, "Mitigation of turbulence induced scintillation using concave mirror in reflection-assisted OOK free space optical links," *Opt. Commun.*, vol. 432, pp. 101–111, Feb. 2019.

[47] Y. Ata and M.-S. Alouini, "HAPS based FSO links performance analysis and improvement with adaptive optics correction," *IEEE Trans. Wireless Commun.*, vol. 22, no. 7, pp. 4916–4929, Jul. 2023.

[48] H. Liu et al., "Turbulence-resistant FSO communication using a few-mode pre-amplified receiver," *Sci. Rep.*, vol. 9, no. 1, 2019, Art. no. 16247.

[49] B. He and R. Schober, "Bit-interleaved coded modulation for hybrid RF/FSO systems," *IEEE Trans. Commun.*, vol. 57, no. 12, pp. 3753–3763, Dec. 2009.

[50] V. Jamali, D. S. Michalopoulos, M. Uysal, and R. Schober, "Link allocation for multiuser systems with hybrid RF/FSO backhaul: Delay-limited and delay-tolerant designs," *IEEE Trans. Wireless Commun.*, vol. 15, no. 5, pp. 3281–3295, May 2016.

[51] H. E. Nistazakis, T. A. Tsiftsis, and G. S. Tombras, "Performance analysis of free-space optical communication systems over atmospheric turbulence channels," *IET Commun.*, vol. 3, no. 8, pp. 1402–1409, 2009.

[52] M. Alzenad, M. Z. Shakir, H. Yanikomeroglu, and M.-S. Alouini, "FSO-based vertical backhaul/fronthaul framework for 5G+ wireless networks," *IEEE Commun. Mag.*, vol. 56, no. 1, pp. 218–224, Jan. 2018.

[53] Y. F. Al-Eryani, A. M. Salhab, S. A. Zummo, and M.-S. Alouini, "Protocol design and performance analysis of multiuser mixed RF and hybrid FSO/RF relaying with buffers," *J. Opt. Commun. Netw.*, vol. 10, no. 4, pp. 309–321, Apr. 2018.

[54] D. Zwillinger and A. Jeffrey, *Table of Integrals, Series, and Products*. Amsterdam, The Netherlands: Elsevier, 2007.

[55] *Unmanned Aircraft Systems—Trial Report*, Qualcomm Technol. Inc., San Diego, CA, USA, 2017.

[56] Y. Huo, X. Dong, T. Lu, W. Xu, and M. Yuen, "Distributed and Multilayer UAV networks for next-generation wireless communication and power transfer: A feasibility study," *IEEE Internet Things J.*, vol. 6, no. 4, pp. 7103–7115, Aug. 2019.

[57] Z. Xiao et al., "A survey on millimeter-wave beamforming enabled UAV communications and networking," *IEEE Commun. Surveys Tuts.*, vol. 24, no. 1, pp. 557–610, 1st Quart., 2022.

[58] J. Ghimire and C. Rosenberg, "Revisiting scheduling in heterogeneous networks when the backhaul is limited," *IEEE J. Sel. Areas Commun.*, vol. 33, no. 10, pp. 2039–2051, Oct. 2015.

[59] Z. Hu, Z. Zheng, L. Song, T. Wang, and X. Li, "UAV offloading: Spectrum trading contract design for UAV-assisted cellular networks," *IEEE Trans. Wireless Commun.*, vol. 17, no. 9, pp. 6093–6107, Sep. 2018.

[60] R. K. Jain, D.-M. W. Chiu, and W. R. Hawe, "A quantitative measure of fairness and discrimination," Eastern Res. Lab, Digit. Equip. Corp., Hudson, MA, USA, Rep. DEC-TR-301, 1984.

[61] A. B. Sediq, R. H. Gohary, R. Schoenen, and H. Yanikomeroglu, "Optimal tradeoff between sum-rate efficiency and jain's fairness index in resource allocation," *IEEE Trans. Wireless Commun.*, vol. 12, no. 7, pp. 3496–3509, Jul. 2013.

[62] A. A. Raja, H. Pervaiz, S. A. Hassan, S. Garg, M. S. Hossain, and M. Jalil Piran, "Coverage analysis of mmWave and THz-enabled aerial and terrestrial heterogeneous networks," *IEEE Trans. Intell. Transp. Syst.*, vol. 23, no. 11, pp. 22478–22491, Nov. 2022.

[63] C. Guo, M. Sheng, X. Wang, and Y. Zhang, "Throughput Maximization with short-term and long-term Jain's index constraints in downlink OFDMA systems," *IEEE Trans. Commun.*, vol. 62, no. 5, pp. 1503–1517, May 2014.
[64] N. Rezaeinia, J. C. Góez, and M. Guajardo, "On efficiency and the Jain's fairness index in integer assignment problems," *Comput. Manag. Sci.*, vol. 20, no. 1, p. 42, 2023.
[65] Q.-V. Pham, S. Mirjalili, N. Kumar, M. Alazab, and W.-J. Hwang, "Whale optimization algorithm with applications to resource allocation in wireless networks," *IEEE Trans. Veh. Technol.*, vol. 69, no. 4, pp. 4285–4297, Apr. 2020.
[66] L. Dong, Z. Liu, F. Jiang, and K. Wang, "Joint optimization of deployment and trajectory in UAV and IRS-assisted IoT data collection system," *IEEE Internet Things J.*, vol. 9, no. 21, pp. 21583–21593, Nov. 2022.
[67] S. M. Bozorgi, M. R. Hajiabadi, A. A. R. Hosseinabadi, and A. K. Sangaiah, "Clustering based on whale optimization algorithm for IoT over wireless nodes," *Soft Comput.*, vol. 25, pp. 5663–5682, Apr. 2021.
[68] P. Singh and S. Prakash, "Optical network unit placement in fiber-wireless (FiWi) access network by whale optimization algorithm," *Opt. Fiber Tech.*, vol. 52, Nov. 2019, Art. no. 101965.
[69] M. Raja, S. Dhanasekaran, and V. Vasudevan, "Opposition based joint grey wolf-whale optimization algorithm based attribute based encryption in secure wireless communication," *Wireless Pers. Commun.*, vol. 27, pp. 635–655, Nov. 2022.
[70] M. Huang, Q. Zhai, Y. Chen, S. Feng, and F. Shu, "Multi-objective whale optimization algorithm for computation offloading optimization in mobile edge computing," *Sensors*, vol. 21, no. 8, p. 2628, 2021.
[71] N. Rana, M. S. A. Latiff, S. M. Abdulhamid, and H. Chiroma, "Whale optimization algorithm: A systematic review of contemporary applications, modifications and developments," *Neural Comput. Appl.*, vol. 32, pp. 16245–16277, Oct. 2020.
[72] S. Mirjalili and A. Lewis, "The whale optimization algorithm," *Adv. Eng. Softw.*, vol. 95, pp. 51–67, May 2016.
[73] A. Kumar, V. Bhalla, P. Kumar, T. Bhardwaj, and N. Jangir, "Whale optimization algorithm for constrained economic load dispatch problems—A cost optimization," in *Proc. Ambient Commun. Comput. Syst.*, 2018, pp. 353–366.
[74] A. J. Kulkarni, E. Mezura-Montes, Y. Wang, A. H. Gandomi, and G. Krishnasamy, *Constraint Handling in Metaheuristics and Applications*. Singapore: Springer, 2021.
[75] T. Plank, E. Leitgeb, P. Pezzei, and Z. Ghassemlooy, "Wavelength-selection for high data rate free space optics (FSO) in next generation wireless communications," in *Proc. 17th Eur. Conf. Netw. Opt. Commun*, 2012, pp. 1–5.
[76] M. Nafees, J. Thompson, and M. Safari, "Multi-tier variable height UAV networks: User coverage and throughput optimization," *IEEE Access*, vol. 9, pp. 119684–119699, 2021.
[77] J. G. Andrews et al., "What will 5G be?" *IEEE J. Sel. Areas Commun.*, vol. 32, no. 6, pp. 1065–1082, Jun. 2014.
[78] J. García-Morales, G. Femenias, and F. Riera-Palou, "Statistical analysis and optimization of a fifth-percentile user rate constrained design for FFR/SFR-aided OFDMA-based cellular networks," *IEEE Trans. Veh. Technol.*, vol. 67, no. 4, pp. 3406–3419, Apr. 2018.

**MUHAMMAD NAFEES** (Member, IEEE) received the B.S. degree in computer engineering from COMSATS University Islamabad (Lahore), Lahore, Pakistan, in 2008, the M.Sc. degree in wireless networks from the Queen Mary University of London, U.K., in 2010, and the Ph.D. degree in electrical engineering from the School of Engineering, The University of Edinburgh, Edinburgh, U.K., in 2024. From 2011 to 2018, he served as a Lecturer with the Department of Electrical and Computer Engineering, COMSATS University Islamabad (Lahore). He is currently a Research Associate with the Institute for Imaging, Data and Communications, The University of Edinburgh. His research interests include unmanned aerial vehicles, fifth-generation and beyond communications, hybrid RF/optical communications, game theory, and machine learning for wireless networks.

**SHENJIE HUANG** (Member, IEEE) received the B.Sc. degree in optoelectronic engineering from Jiangnan University, Wuxi, China, in 2013, and the M.Sc. degree in signal processing and communications and the Ph.D. degree in electrical engineering from The University of Edinburgh, Edinburgh, U.K., in 2014 and 2018, respectively, where he is currently a Research Associate with the Institute for Imaging, Data and Communications. His main research interest is in free-space optical communications.

**JOHN THOMPSON** (Fellow, IEEE) is currently the Personal Chair of Signal Processing and Communications with the School of Engineering, The University of Edinburgh. He also specializes in antenna array processing, energy-efficient wireless communications, and more recently in the application of machine learning to wireless communications. To date, he has published in excess of 500 journals and conference papers on these topics. He is also an Area Editor of the wireless communications topic in IEEE TRANSACTIONS ON GREEN COMMUNICATIONS AND NETWORKING. In January 2016, he was elevated to a fellow of the IEEE for research contributions to antenna arrays and multihop communications. He was also one of four scientists elevated to fellow of the European Association for Signal Processing in 2023, for "Signal Processing Advances in Multiple Antenna and relayed Wireless Communication Systems."

**MAJID SAFARI** (Senior Member, IEEE) received the B.Sc. degree in electrical and computer engineering from the University of Tehran, Iran, in 2003, the M.Sc. degree in electrical engineering from the Sharif University of Technology, Iran, in 2005, and the Ph.D. degree in electrical and computer engineering from the University of Waterloo, Canada, in 2011. He is currently a Professor with the Institute for Imaging, Data and Communications, University of Edinburgh. Before joining Edinburgh in 2013, he held postdoctoral fellowship with Mc-Master University, Canada. His main research interest is the application of information theory and signal processing in optical communications including fiber-optic communication, free-space optical communication, visible light communication, and quantum communication. He is also an Associate Editor of the IEEE TRANSACTIONS ON COMMUNICATIONS and was the TPC Co-Chair of the 4th International Workshop on Optical Wireless Communication in 2015.